Examensarbete
TVVR 08/5004

Impact on the coastal areas of the Tanjung Tokong Land Reclamation Project, Penang, Malaysia

Effects on wave transformation, sediment transport, and coastal evolution

Salwa Ramly

Division of Water Resources Engineering
Department of Building and Environmental Technology
Lund University

Avdelningen för Teknisk
Vattenresurslära
ISRN LUTVDG/TVVR-08/5004
ISSN-1101-9824

Impact on the coastal areas of the Tanjung Tokong Land Reclamation Project, Penang, Malaysia

Effects on wave transformation, sediment transport, and coastal evolution

By:
Salwa Ramly

Supervisor: Professor Magnus Larson

Examiner: Professor Hans Hanson

LTH, Lund University
January 2008

Acknowledgements

The success of this Master Thesis is to a large extent due to all of the people who helped me during the course of this work.

At this opportunity, I would like to express my sincere thanks to my supervisor, Professor Magnus Larson, from Department of Water Resources Engineering, LTH, who helped me throughout the whole process, with advice and detail explanations on the subject. I appreciate, very much, the time spent on me and the opportunity to acquire new knowledge in my study.

I would like to thank the Department of Irrigation and Drainage (DID) Malaysia, DID Penang and Malaysian Meteorology Department for the data, references and valuable information that have been used in this study. Special thanks to Ir Teoh Boon Pin, from the Coastal Section, DID Malaysia, for the help regarding the project.

Thanks also to Hoan Le Xuan and Thanh Nam Pham, Doctoral Students at the Department of Water Resources Engineering, LTH, for the help on the EBED Model and MATLAB Programming in this study.

In appreciation of the EBED Model, I would like to thank Professor Hajime Mase, from the Disaster Prevention Research Institute, Kyoto University, Japan for his effort to develop EBED Model which was used in this study.

Also thanks to the Public Services Department of Malaysia and Department of Irrigation and Drainage Malaysia, for giving me the opportunity to further my study at Lund University.

And last but not least, thank you very much to my beloved family for great support and always being a source of encouragement and energy.

Abstract

Rapid development in urban areas of maritime countries may need solutions to address scarcity of land for development and infrastructure. Land reclamation has been an option in many maritime countries, including in Malaysia to overcome this problem. Tanjung Tokong Land Reclamation Project is an ongoing development project in Penang, Malaysia, where housing and commercial properties are constructed on the reclaimed area. The main objective of this study is to determine the effect of the Tanjung Tokong Land Reclamation project on the coastal areas regarding wave transformation, sediment transport, and coastal evolution. However, the effects on the environment and ecosystems are not included. Initially, general coastal processes in Penang were investigated and the project background described to get an overview of the study area. Then, a numerical model, EBED, was employed to simulate the nearshore wave transformation in the specified study area for four different scenarios of incident wave heights and wave directions before and after the project. Based on the EBED simulation results, changes in the wave transformation pattern after the land reclamation project were assessed. Wave transformation for incoming waves from the west was more significantly affected compared to incoming waves from the north and east by the land reclamation. Local sediment transport rates also changed after the project, mainly because of the influence on the incoming local wave height and direction. However, there were no significant differences concerning the local sediment transport direction along the coast after project. The effects on the coastal evolution of the project were increased erosion for waves coming from the west and increased accumulation for waves coming from the east side for particular stretches of coastline in the vicinity of the project site. As an overall conclusion, this study showed that the Tanjung Tokong Land Reclamation Project have an impact on the wave transformation, sediment transport, and evolution of the coastal areas in the vicinity of the land reclamation, but there is limited impact some distance away from the project site.

Keywords: *land reclamation, wave transformation, sediment transport, coastal evolution, EBED Model*

Table of Contents

1. Introduction

1.1 Background

Figure 1 : Tanjung Tokong Land Reclamation Project in Penang, Malaysia

Land reclamation has played a significant role in the urban development process in the coastal areas of many maritime countries. Population growth typically demands more area for development and infrastructure. Many maritime countries such as Singapore, Hong Kong, and Japan regard beach reclamation as an important path to solve scarcity of land. The same situation prevails in Malaysia, especially in Penang.

Penang or Pulau Pinang is located on the north-west coast of Peninsular Malaysia. It is famous among tourist as an attractive island and a modern developed city. Penang has experienced rapid development as a result of positive economical growth. The demand of urban development and infrastructure has increased accordingly with the population growth in the state. As a result, scarcity of land has become one of the main problems in Penang. Shortage of land in Penang, especially in the northeast part of the island, made the state government approve the Tanjung Tokong Land Reclamation Project. Figure 1 shows the ongoing construction project for housing at Tanjung Tokong Land Reclamation Project located in the northeast of Penang.

The land reclamation is expected to impact the coastal hydraulics, environment, and ecosystems. In the present study, an investigation on the impact of the Tanjung Tokong Land Reclamation Project, Penang, Malaysia, on the coastal areas was carried out and the result is presented in this report. The study was conducted to assess the effects on wave transformation, sediment transport, and coastal evolution, whereas the effects on environment and ecosystems are not included. General coastal processes are described and a project background is first provided in the report. Then, wave conditions and nearshore sediment transport are discussed in detail and the effects of the land reclamation are highlighted before the conclusions are presented.

1.2 Objectives

By understanding coastal processes in general and the wave transformation along the shore in particular, the effects of the land reclamation may be determined. The main objectives of this study are:

- To identify the impact on the wave transformation due to the Tanjung Tokong Land Reclamation Project
- To determine the general pattern of the sediment transport in the area and to quantify the transport, as well as the changes in sediment transport occurring in response to the land reclamation project
- To forecast the coastal evolution after the land reclamation project

1.3 Procedure

In order to carry out this study, relevant literature was studied to get an understanding of coastal and wave processes in general of importance for the study area. Available technical reports from the Tanjung Tokong Land Reclamation Project were studied to gather all information regarding the project. In addition, specific information on project area and coastal processes in Penang, as well as available data, were compiled from the literature and through contacts in Penang.

Different types of data were used in this study such as sea charts, wind data, wind statistics, and wave statistics, which were collected from various sources. The wave data were obtained from the Department of Irrigation and Drainage, Penang, as well as from Department of Irrigation and Drainage, Malaysia. Wind data were provided by the Department of Meteorology, Malaysia. Sea charts (based on British Admiralty Charts) were purchased by the Department of Water Resources Engineering, LTH, from the National Oceanic and Atmospheric Administration (NOAA). These sea charts were utilized to develop a bathymetry map as a base map for study area.

Specialized computer programs were employed in this study to carry out simulations and calculations tasks. A FORTRAN program was developed for the wave hindcasting, where four years of wind data were used to obtain a representative wave climate for northern Penang and the study site. The wind data consisted of wind speed and direction for every hour from the 1st of January 2003 to the 31st of December 2006.

Two bathymetric data set were used in this study, before the project and after the project. For before the project, the bathymetric data were based on sea charts, where the British Admiralty Chart No 71058 was used to develop the bottom topography for the wave transformation simulations. The SURFER program was used to digitize the map and MATLAB programs were used to interpolate the bathymetric map for the study area for condition before the project. Since bathymetric survey after the project was not available, bathymetric map for the study area after the project was made by modify the land boundary of the first bathymetric map based on the land reclamation project layout.

A numerical wave transformation model, the EBED Model, was used to simulate nearshore wave conditions in the study area. The model was run for four representative scenarios of incident wave height and wave direction to simulate the wave transformation at the study site. There were two cases for each scenario, before and after the land reclamation project. Comparisons of wave transformation were made for conditions before and after the project for every scenario.

Breaking wave parameters were determined from the EBED output in the nearshore to calculate the alongshore sediment transport rate. By determining the sediment transport rate and its direction, the coastal evolution with regard to either erosion or accumulation was predicted for the coastal areas before and after the land reclamation project.

In addition, the regional sediment transport pattern along the northern part of the Penang Island was calculated to obtain a general overview of the sediment transport pattern in the area and the availability of sediment along the coastline for transport to the study area.

2. Coastal Processes at Penang, Malaysia

2.1 Climatic conditions

Figure 2 : Map of Malaysia which is located in the equator region surrounded by South China Sea and Straits of Malacca.

Malaysia is a tropical country and subjected to influence by the sea. The characteristic description of the climate of Malaysia is uniform temperature, high humidity, and plenty of rainfall. In general, mean daily temperature ranges from 21^{o}C to 32^{o}C throughout the year and the average annual rainfall from 1,500 mm to 4,000 mm. Since Malaysia is situated in the equator region, it is cloudy and sunny most of the time. It is rare to have a full day with completely clear sky without clouds, even in periods of severe drought. On the other hand, it is also uncommon to have a stretch of a few days with no sunshine, except during the northeast monsoon season. Winds in Malaysia are generally light originating in the Andaman Sea and the South China Sea. Since Penang is located on the west coast of Peninsular Malaysia, winds from the Andaman Sea and the Straits of Malacca are more influential for the wind conditions at Penang.

There are two common monsoon seasons, the southwest monsoon and the northeast monsoon, as well as two shorter inter-monsoon seasons. The southwest monsoon is usually established in the end of May or early June and ends in September and the wind flow is generally from southwest. The northeast monsoon typically begins in early

November and ends in March and steady winds blow from northeast and northwest. The winds during the two inter-monsoon seasons are generally light and variable.

Appendix 1 and 2 show the annual and monthly wind rose summaries at Butterworth Meteorological Station, which is the nearest meteorological station to project area. This station is located on the mainland and opposite to the project area. Winds are measured at an elevation of 2.8 meter above mean sea level. These wind rose summaries can be use to get an overall picture of the wind conditions at Penang.

In general, the annual wind rose summaries in Appendix 1 suggest that the wind speed at this station is basically less than 8 m/s. More than 12% winds blow from northwest and northeast directions.

In Appendix 2 the monthly wind rose summaries show that Butterworth Meteorological Station experienced more winds from northwest direction throughout the year with more than 12% winds blow from northwest direction. Constant winds from the Andaman Sea with the larger fetch length caused more winds from northwest direction at this station compared to other directions.

However, the monsoons are also of importance for the wind direction. During the northeast monsoon, November to March, more winds blow from the northeast and east directions. Meanwhile, during the southwest monsoon, May to September, wind directions from southwest and west are more significant after the northwest direction. For inter monsoon seasons, April and October, more than 15% of the winds blow from the northwest direction in 24 hours and relatively less winds blow from other directions.

Four years wind data series, year 2003-2006 were used in the wave hindcasting. The details of the wave calculations will be discussed in section 4, Wave Conditions.

2.2 Hydrodynamic conditions

The water level changes caused by tidal motion are significant at Penang Island. Based on Tide Table Malaysia, the difference between MHWS and MLWS is 2.0m (see Table 1 for abbreviations). Tide elevations at Penang is summarized in Table 1.

Table 1: Tidal Elevation at Penang

Highest Astronomical Tide (HAT)	+3.3 m ACD
Mean High Water Spring (MHWS)	+2.6 m ACD
Mean High Water Neap (MHWN)	+1.8 m ACD
Mean Sea Level (MSL)	+1.6 m ACD
Mean Low Water Neap (MLWN)	+1.3 m ACD
Mean Low Water Spring (MLWS)	+0.6 m ACD
Lowest Astronomical Tide (LAT)	+0.0 m ACD

Note: ACD is Admiralty Chart Datum

In general, there are four types of currents in the Strait of Malacca, longshore currents generated by breaking waves, tidal currents generated by tides, surface currents generated by winds, and currents generated by discharge from rivers. Surface currents generated by wind are small and because of limited wave action the longshore current is significant only close to shore. Tides dominate the hydrodynamics in the open sea area, and only tidal currents have significant influence on the flow conditions in the Strait. In general, the current flows southwards during flood tide and northwards during ebb tide. From previous studies in this area, the average tidal current during spring period is 0.4 m/s and 0.1 m/s during neap period. In the nearshore area, however, the tidal currents are small due to frictional effects. In theses areas, the longshore currents generated by breaking waves are dominant with implications for the nearshore sediment transport. Predominant directions of tidal currents are 315^o to 355^o (from North) during ebb and 135^o to 170^o (from North) during flood tide. Current velocities are stronger during spring period with maximum speed 1.0 m/s (TPD, 2003).

Based on previous studies (TPD, 2003) it was observed that the sediment concentration offshore of Tanjung Tokong were higher than the sediment concentration in offshore area near Georgetown. Sediment concentration at Tanjung Tokong area varied being 200 g/m^3 during spring tide and 50 g/m^3 during neap.

Bed materials within the bay are mostly very fine silt material with mean grain size in the range of 0.0015mm to about 0.1mm. West of Tanjung Tokong, bed materials are coarser with a mean grain diameter in the range of 0.2mm to 0.3 mm (TPD, 2003).

Wave statistic summaries for Penang from the 1st of January 1968 to the 31st of December 1984 are presented in Appendix 3. These data were provided by the Coastal Engineering Division, Department of Irrigation and Drainage, Malaysia. The wave statistic summaries are based on ship observations. Wave statistic summaries show that the waves from directions 285 degrees to 315 degrees have the highest index for wave height and wave period followed by directions 255 to 285 degrees and directions 315 to 345 degrees. It seems that waves from southwest to northwest have higher wave heights compared to the other directions. Offshore waves are relatively low in height with most of the waves have heights less than 0.75 meter. However, there are a few cases with wave heights being greater than 1.0 meter.

3. Tanjung Tokong Land Reclamation Project

3.1 Project description

Tanjung Tokong Land Reclamation Project, Penang, Malaysia, is a development project which is carried out with the Tanjung Pinang Development Sdn. Bhd. (TPD) as the developer. TPD was awarded a concession by the State Government of Penang to reclaim and to develop 971,000 m^2 of coastal area in Tanjung Tokong for commercial and residential use. The proposed site is located at 5^o 27' N and 100^o17' E and situated 5 km north west of Georgetown, the capital city of Penang. The reclaimed offshore area is 5 km along the coast between Tanjung Tokong and Gurney Drive and fronting seawards the North Channel as shown in Figure 3.

Figure 3 : Tanjung Tokong Land Reclamation Project

The total land reclamation area is about 971,000 m^2 and the amount of fill material is approximately 4,000,000 m^3 (TPD, 2003). A breakwater that is 265 meter long is being built to trap the longshore sediment coming from the north. Also, a marina is constructed in the northeast part of the reclamation area, and water edge areas are created for the bungalows in the southeast part of the reclamation area.

The reclamation works was carried out in year 2004 and it was finished in 2006. Currently development work, such as build housing and commercial buildings, is in progress. Figure 4 shows a view of the project area.

Figure 4 : View of the Tanjung Tokong Land Reclamation Project (from Google Earth)

3.2 Location and site description

Tanjung Tokong Headland is located at the northern end of the project area. The coastline of the project area is sheltered by this headland and the shallow bay between Tanjung Tokong Headland and Gurney Drive, Georgetown. From Figure 5 it is clearly seen that between the northern and southern limits of the reclamation site, the coastline has a natural circular, curve shape. Furthermore, the coastline is straight along the Bagan Jermal until Gurney Drive in the southern part of the study area. In general, this shallow bay is exposed during low tide. The area is facing siltation due to the shape of the headland of the Tanjung Tokong and being exposed to the largest waves from the sea coming out of the northwest. In the previous hydraulic study (TPD, 2003), it was reported that a sand spit formed at the northern end of the land reclamation site extending seawards about 950 meter long and 50 meter wide indicating that siltation occurred in this area.

The coastline of the project site is covered with sandy beaches in the central portion and a mixture of silty sand and soft clay in the northern and southern part of the area. Offshore material is mainly mud except at certain pockets where the sand particles are found.

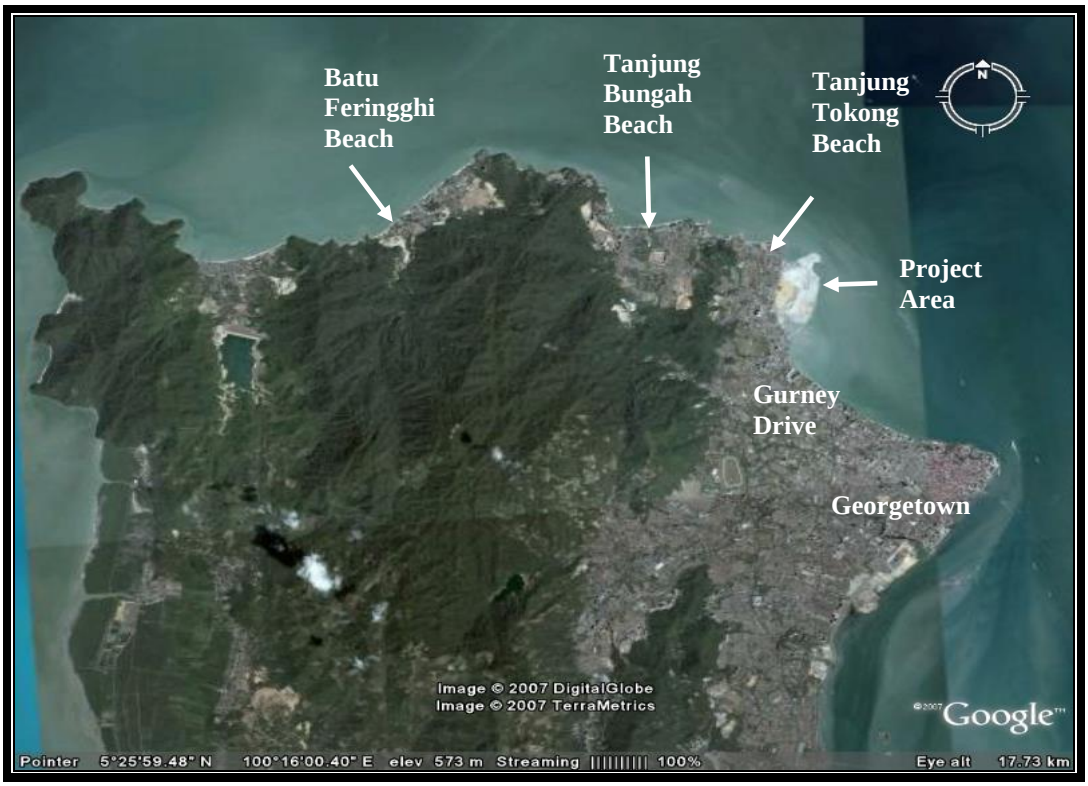

Figure 5 : North part of Penang Island

Figure 5 shows the location of the beaches along the northern part of Penang Island. There are sandy beaches from the west side of Tanjung Tokong along the north part of Penang Island. Most of the beaches are located between rocky headlands. These beaches have become attractive tourist areas and there are many hotels available along these beaches.

Tanjung Tokong Beach, which is located immediately west of Tanjung Tokong headland, can be categorized as a moderately exposed sandy beach with medium to fine sand. Shell debris can be found easily on the foreshore of this beach. The water is often turbid indicating a relatively high content of suspended sediments.

Tanjung Bungah Beach which is situated between the two next headlands to the west is also a moderately exposed sandy beach with medium sand, slightly coarser than the sand on the Tanjung Tokong Beach. However, there is not so much shell debris on this foreshore and the water is also turbid.

A few kilometers further northwest of the Tanjung Bungah Beach, there is a famous beach called Batu Feringghi Beach. The beach sand is coarser and can be categorized as medium to coarse sand. This beach is potential sediment supply for sediment transport in the North Channel of the Strait of Penang. However, this study will only cover the beaches from Tanjung Bungah until Gurney Drive. The boundaries of the present study area for assessing the impact of the land reclamation is smaller than this coastal stretch and is shown in Figure 6.

The offshore area of the project site includes the Straits of Penang, which is separating the island of Penang and the mainland of Peninsular Malaysia. The Straits of Penang encompasses a narrow and deep channel with 16 meter depth. This channel is relatively busy with ship traffic since it is the main entrance to Penang Harbor. In general, the offshore contours are aligned with the coastline of Penang Island and also with the mainland, as can be seen in Figure 6.

Along Penang Island, close to the coastline, the gradient of the seabed is gentle. The slope is 1:900 towards the sea until the 2 meter contour is encountered. From the 2 meter contour, the slope drops to 1:300 until the 5.0 meter contour and more steeply with 1:180 gradient at the deepest end towards the 16-meter depth, before climbing again with a gentler slope towards the mainland. The main channel within the 10 meter contour is about 240 meter wide.

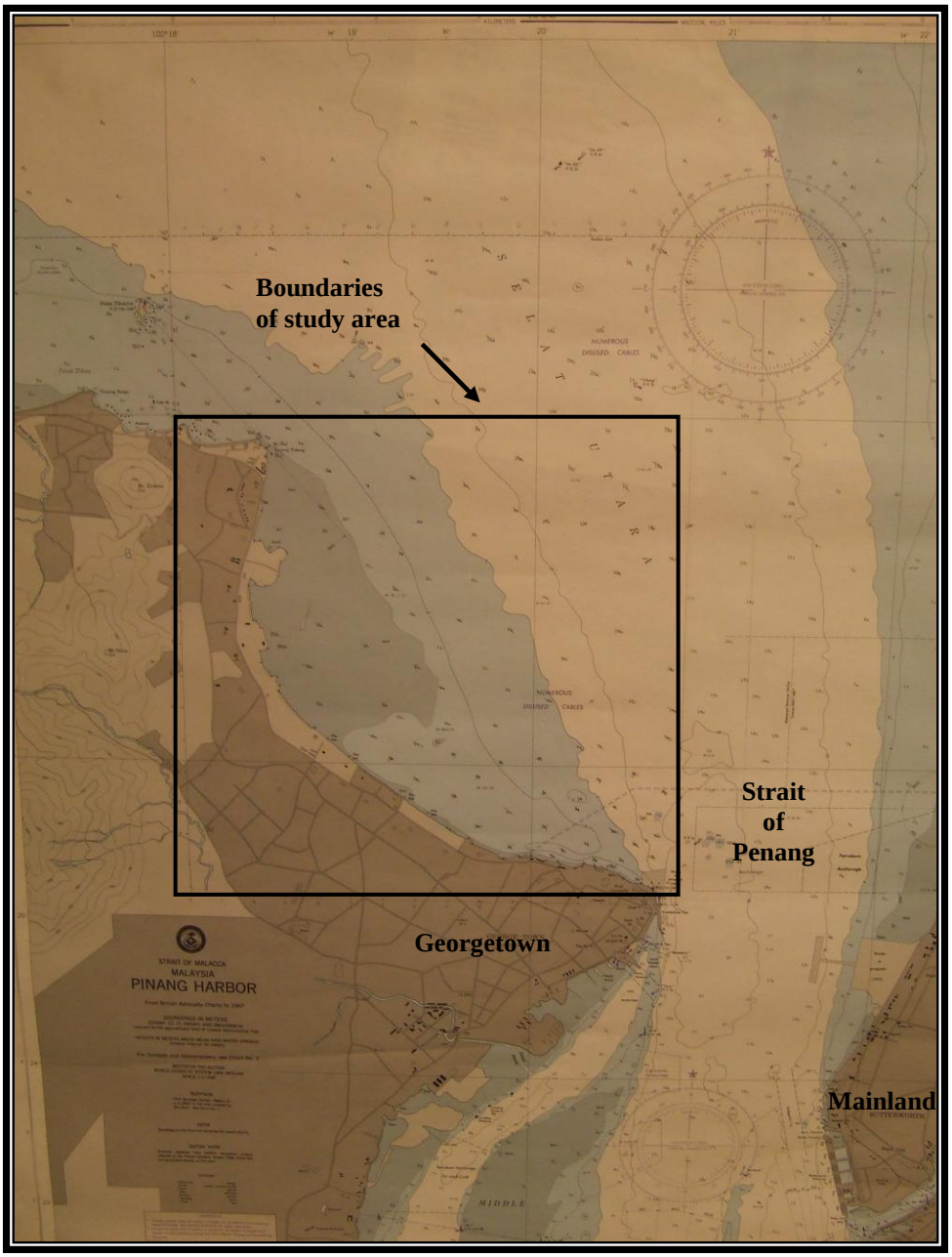

Figure 6 : Boundaries of study area for impact of the land reclamation and Strait of Penang separating Penang Island and Peninsular Malaysia

4. Wave Conditions

4.1 Offshore waves

There are three factors that influence the offshore waves generated by wind. These are wind speed, wind duration, and fetch length. To generate a specific set of offshore waves, a certain time period of wind action known as wind duration is required in combination with the distance along which the wind is acting in the particular direction, called fetch length. When the wind blows with a certain speed over the sea surface, the wind will transfer energy to the sea. The wave will increase in height and period as long as the wind blows, up to some limiting values. When the waves travel faster than the wind speed, the waves will reach their limiting condition (SPM, 1984).

When the wind is unable to transfer all its potential energy to the waves, the wave field will not be fully developed. There are two conditions determining wave fields that are not developed, that is, fetch-limited or duration-limited conditions. Fetch-limited condition will happen when the wave height reaches equilibrium at the end of the fetch with the wind blowing continuously and consistently. However, for duration-limited condition, the duration of the wind blowing is not long enough to generate an equilibrium situation, which will cause the wave height to be limited, even though the wave is still not at the end of the fetch (SPM, 1984).

If the waves reach their largest height for a specific wind speed, wind duration, and fetch length the wave field becomes fully developed. This means that any increase in wind speed or wind duration for a particular direction will not increase the wave height. Even for the open sea with no limit on the fetch length and for infinite wind duration, a maximum wave height will develop for a particular wind speed, since the wave growth eventually will be limited by dissipative processes.

Offshore wave prediction based on past meteorological conditions is known as wave hindcasting. As discussed above, the important parameters in wave hindcasting are wind speed, wind duration, fetch length, and the average depth of the sea (affects the energy dissipation). Wave hindcasting are normally done using a computer program or a more sophisticated numerical model (SPM, 1984).

In this study, wave hindcasting was carried by using the wind data series from the Butterworth Meteorological Station, which is the nearest meteorological station for the study area. This station is situated in the mainland of Peninsula Malaysia and opposite to the project site. The wind data consist of wind speed and wind direction every one hour from the 1st of January 2003 until the 31st of December 2006.

The wind waves were hindcasted using a specially developed computer program written with in FORTRAN program language. The input data for this program are wind speed, wind direction, fetch length, and also the average water depth along the fetch length. In

this program, wind speed and direction were assumed to be constant during one hour until next wind record was made.

Estimation of surface winds for wave prediction was made based on SPM (1984). The wind is assumed to be driven by large-scale pressure gradients in the atmosphere that have been in a near steady state. At 1000 m above the water surface, the winds are driven mainly by the geostrophic balance between Coriolis and local pressure gradient forces. Below this level, the wind field is distorted by frictional effects. This cause the wind speed and direction to be dependent on the elevation above the mean surface, roughness of the surface, air sea temperature differences, and horizontal temperature gradients (SPM 1984). Hence, there are five adjustment factors that can be applied to measured wind data. These factors are gage elevation, duration-average wind speed, air-sea temperature stability correction, gage location effects, and coefficient of drag.

The correction factor for elevation difference is typically the most important one to consider. Wind speeds must be adjusted if the winds are not measured at 10 meter elevation, which is the standard elevation for input winds to wave prediction models. If the gage elevation is not more than 20 meter, following equation can be use for wind speed adjustment:

$$U(0) = U(z)\left(\frac{10}{z}\right)^{1/7} \qquad (4.1)$$

In equation (4.1) z is the observed elevation for the wind data. The wind data at Butterworth Station are measured at an elevation of 2.8m above the mean sea level. Therefore, the corrections for elevation difference were made accordingly. There were no corrections made with regard to air-sea temperature stability, duration-average wind speed, and gage location.

The wave growth formulas are expressed in terms of the wind stress factor U_A also known as the adjusted wind speed. The wind stress factor account for the nonlinear relationship between wind stress and wind speed U in m/s and is expressed as:

$$U_A = 0.71U^{1.23} \qquad (4.2)$$

The spectral wave height H_{m0} and peak spectral period T_m of the waves in deep water can be predicted from the known adjusted wind speed. For deep water conditions, the relative water depth, h, over wavelength, L, or h/L, is greater than 0.5 and the wave characteristics are independent of the water depth (SPM, 1984). To predict waves in deep water under fetch-limited wind conditions, the required parameters are the wind stress factor U_A and the fetch length, F, according to,

$$H_{m0} = 5.11 * 10^{-4} U_A F^{1/2} \qquad (4.3)$$

$$T_m = 6.23 * 10^{-2} \left(U_{AF} \right)^{1/3} \qquad (4.4)$$

$$t_m = 32.15 \left(\frac{F}{U_A} \right)^{1/3} \qquad (4.5)$$

where H_{mo} is the spectral wave height, T_m is the peak spectral period, and t_m is the duration needed for fetch-limited conditions to be attained. The calculated H_{mo} and T_m also need to be check so that they are not exceeding the value for fully developed sea:

$$H_{m0} = 2.48 * 10^{-2} U_A^{\ 2} \qquad (4.6)$$

$$T_m = 0.83 U_A \qquad (4.7)$$

$$t_f = 7.296 * 10^3 U_A \qquad (4.8)$$

If the duration of the wind t_v is shorter than the time it takes for the wind to travel the fetch length t_m, which implies that equilibrium is attained, then the waves are duration-limited. Under duration-limited conditions the wave heights are limited by the time the wind has blown. As stated earlier, it is assumed that the winds blow at a constant speed over the one-hour time interval, (t_v) between two consecutive records.

If the waves are duration-limited (t_v<t_m) an imaginary fetch length could be calculated by substituting the duration t_v with U_A in equation 4.5. This imaginary fetch length can then be used to calculate H_{mo} and T_m from equation 4.3 and 4.4, for duration-limited conditions. However, here a slightly approach will be taken based on an evolution equation for the wave height that will describe wave growth and decay in a better manner compared to the SPM method.

The wavelength for deep water is given by,

$$L_o = \frac{gT^2}{2\pi} = 1.56T^2 \qquad (4.9)$$

where T is the period of the waves and g is the acceleration due to gravity. The deep water phase speed C_o and group speed C_{go} are:

$$C_o = \frac{L_o}{T} \qquad (4.10)$$

$$C_{g,o} = \frac{1}{2} C_o \qquad (4.11)$$

Wave predictions from wind can be done empirically for shallow water conditions (Emanuelsson and Mirchi, 2007). For shallow water conditions, the water depth affects the wave generation because of increased energy dissipation. For a given set of wind and fetch conditions, wave heights will be smaller and wave periods shorter, if the generation takes place in transitional or shallow water rather than in deep water (SPM, 1984). In shallow water, bottom friction and percolation in the permeable sea bottom will reduce the wave height and shorten the wave period. The following equations are given for waves generated in shallow water, where equation 4.18 is used in the same way as equation 4.5, to find out if the waves are fetch-limited or duration limited:

$$\frac{gH_{mO}}{U_A^{\,2}} = 0.283 \tanh\left(K_1\right) \tanh\left(\frac{K_2}{\tanh\left(K_1\right)}\right) \qquad (4.12)$$

$$\frac{gT_m}{U_A} = 7.54 \tanh\left(K_3\right) \tanh\left(\frac{K_4}{\tanh\left(K_3\right)}\right) \qquad (4.13)$$

$$K_1 = 0.53\left(\frac{gH}{U_A^2}\right)^{3/4} \qquad (4.14)$$

$$K_2 = 0.565\left(\frac{gF}{U_A^2}\right)^{1/2} \qquad (4.15)$$

$$K_3 = 0.833\left(\frac{gh}{U_A^2}\right)^{3/8} \qquad (4.16)$$

$$K_4 = 0.0379\left(\frac{gF}{U_A^2}\right)^{1/3} \qquad (4.17)$$

$$\frac{gt_m}{U_A} = 537\left(\frac{gT_m}{U_A}\right)^{7/3} \qquad (4.18)$$

A method that takes into account the wave evolution at the previous time step was employed to improve the wave predictions and to better take into account wave growth and decay (Dahlerus and Egermayer, 2005):

$$\frac{dH}{dt} = \varphi\left(H_{eq} - H_{in}\right) \qquad (4.19)$$

Equation (4.19) was used to improve the wave prediction by considering the wave conditions at the beginning of a certain time step for which the SPM equations were employed. The *dH* is the wave height change that occurs during a small time *dt*, φ is a constant, H_{eq} is the equilibrium height according to SPM (1984), and H_{in} is the wave height from the previous time step. Using equation 4.19 the wave will grow or decay from the wave height of the previous time step according to,

$$H = H_{eq} - \left(H_{eq} - H_{in}\right) e^{-\mu \frac{t}{t_{lim}}} \qquad (4.20)$$

where t_{lim} is the limiting duration (taken equal to t_m), t is the duration of the wind measurement (1 hr in the present case), and μ is a constant, which is determined by a least-square fit method to the SPM wave growth function. If the wind changes and start to approach from a direction which can not generate any waves the waves will decay towards zero and have the same direction as the last waves that could be generated by the wind. The same type of relationship for the wave height as given by equation 4.20 was also assumed to be valid for the wave period.

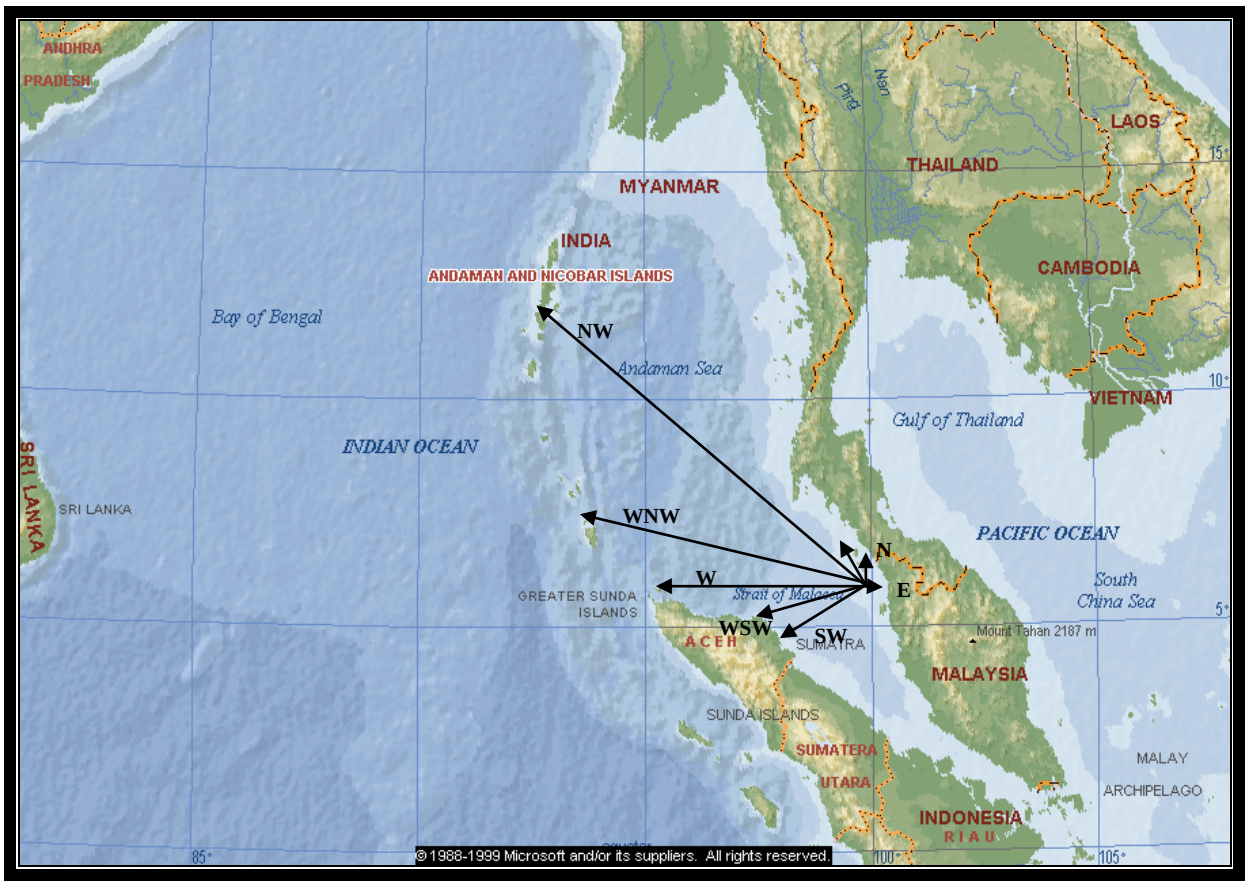

Figure 7: Fetch lengths in the study area.

The fetch lengths, water depths, and wind data were used as input data to the computer program, which encompassed equations (4.2) – (4.20), to generate offshore waves. Figure 7 shows the fetches of interest in the study area. The fetch lengths were measured using a sea chart and also the geographic software Encarta 2000. Strong winds are expected from northwest for which the winds blow across the Andaman Sea. A summary of the fetch lengths and water depths are provided in table 2.

Table 2: Wind direction, average water depth, and fetch length in the study area

Wind Direction	Fetch Length (km)	Average Water Depth (m)
ESE	13	9
E	12	7
ENE	11	6
NE	12	6
NNE	90	8
N	80	10
NNW	100	13
NW	1000	870
WNW	800	500
W	480	40
WSW	260	30
SW	250	25

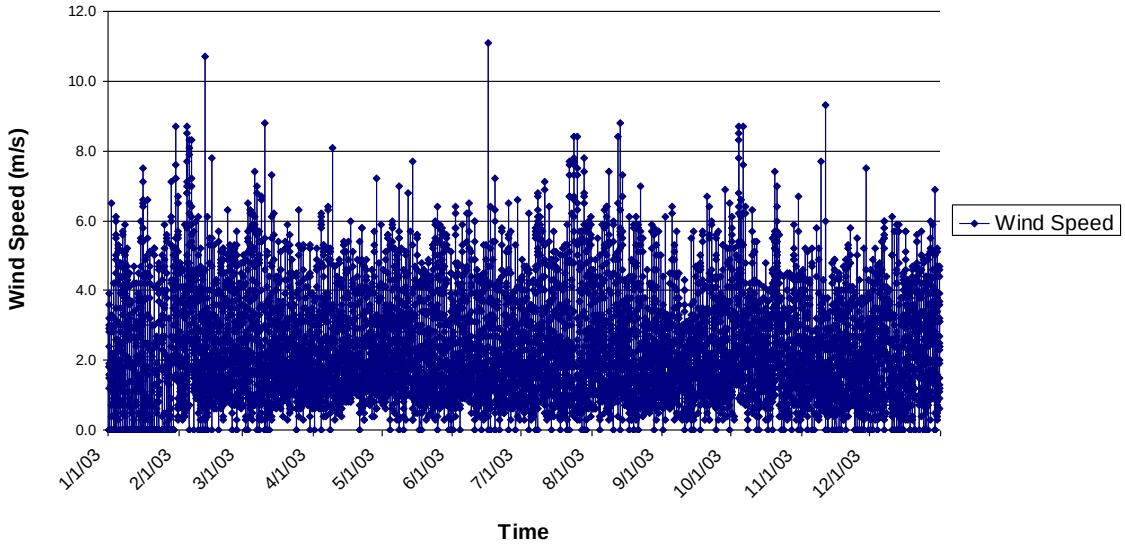

Figure 8 : Wind speed for year 2003 at Butterworth Meteorology Station

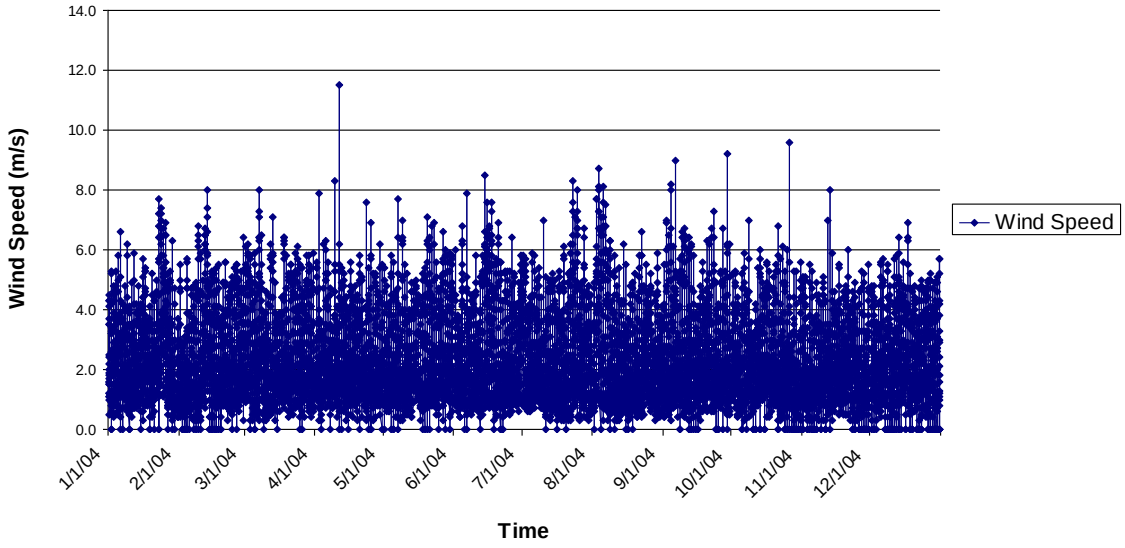

Figure 9 : Wind speed for year 2004 at Butterworth Meteorology Station

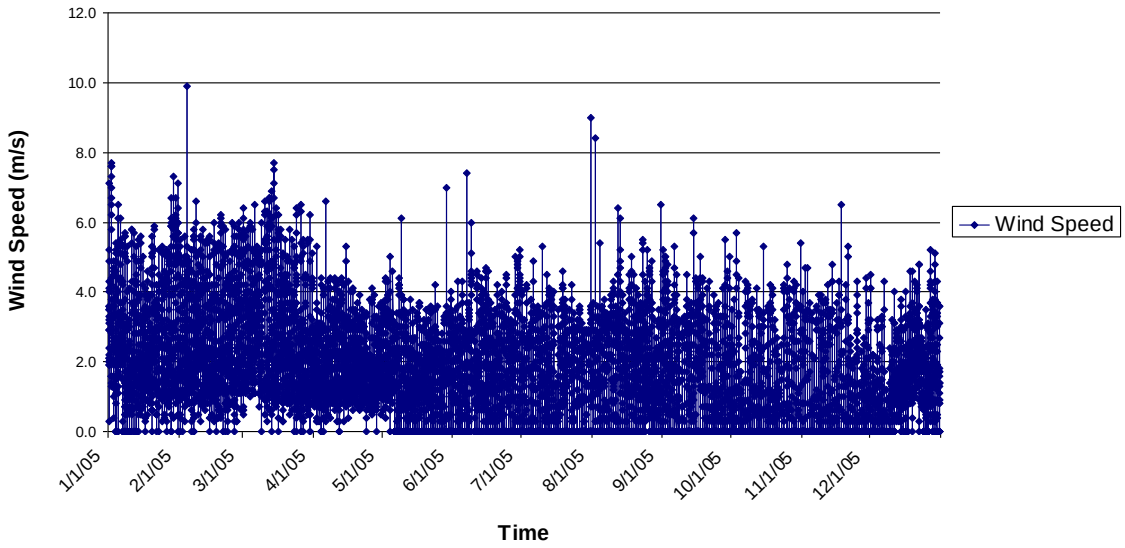

Figure 10 : Wind speed for year 2005 at Butterworth Meteorology Station

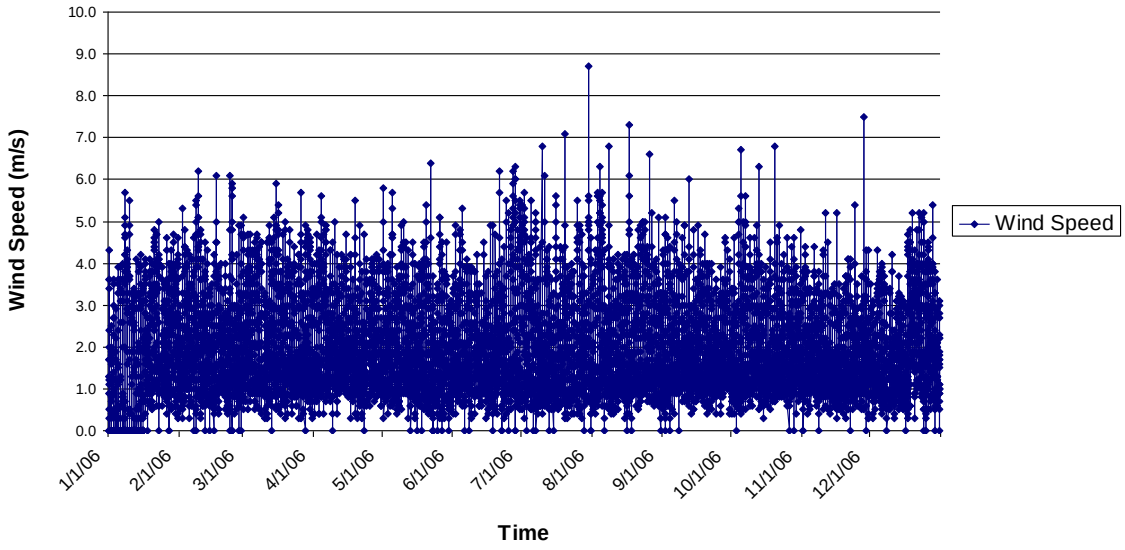

Figure 11 : Wind speed for year 2006 at Butterworth Meteorology Station

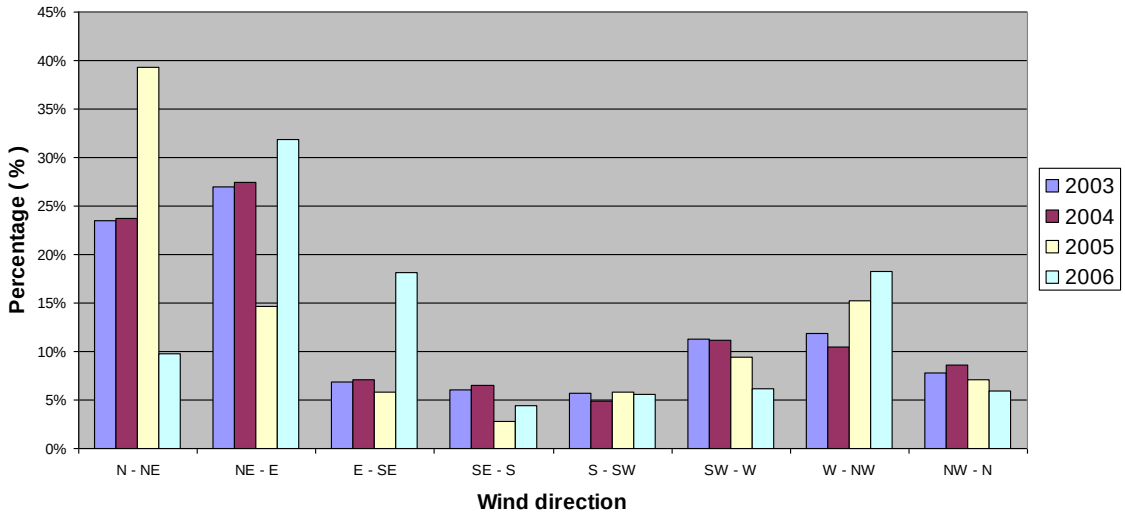

Figure 12 : Summaries of wind direction at Butterworth Meteorology Station

Figure 8 to Figure 11 show the wind speed at Butterworth Meteorology Station for the years 2003, 2004, 2005, and 2006. These wind data was used to hindcast offshore waves. It can be seen that the average wind speed at this station was less than 8 m/s, but occasionally it could reach 10 m/s. The average wind speed for these four years of wind data for all directions is 2.1m/s. Based on these data it was concluded that the wind speed for this location is relatively mild and not so much fluctuating throughout the year. For

this data set, the highest wind speed is 11.5 m/s and this event occurred on the 11th of April, 2004.

Figure 12 shows a summary of the wind direction at Butterworth Meteorology Station for year 2003 to 2006. From this figure, the winds from the northeast region show the highest percentage of occurrence for all four years and the lowest percentage of wind direction is obtained for the south region.

These figures were compared with the wind rose summary diagrams in Appendix 1 and 2 and in general the similarity is significant. Therefore this data set should be acceptable to use to hindcast the offshore wave climate.

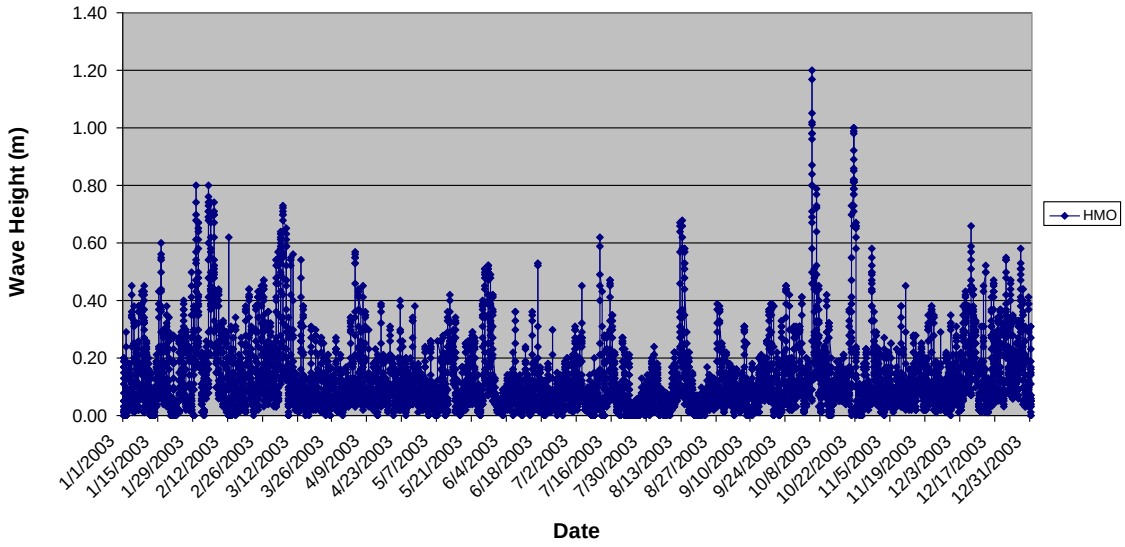

Figure 13 : Offshore waves height for year 2003

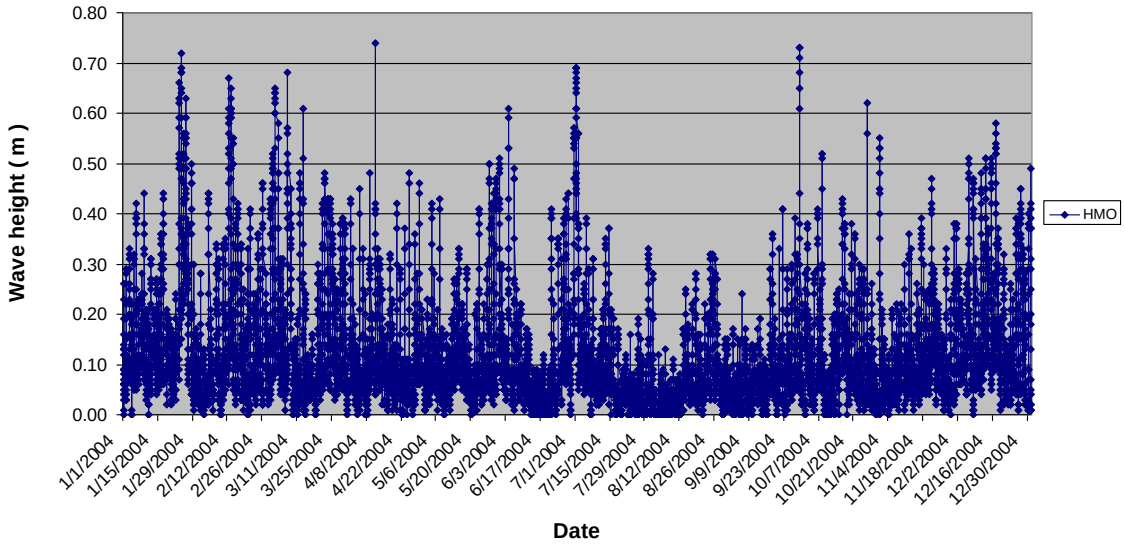

Figure 14 : Offshore waves height for year 2004

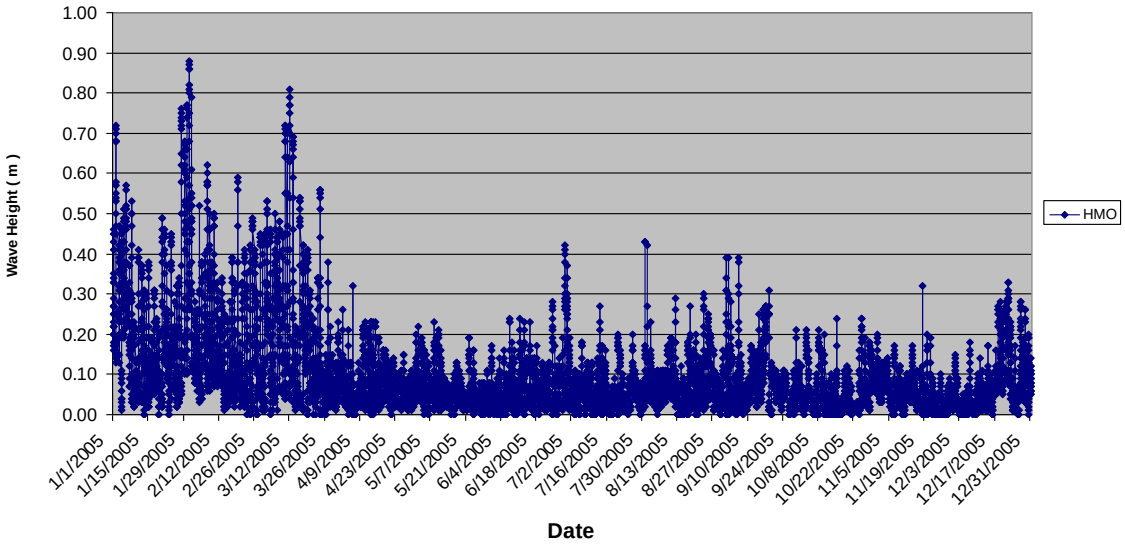

Figure 15 : Offshore waves height for year 2005

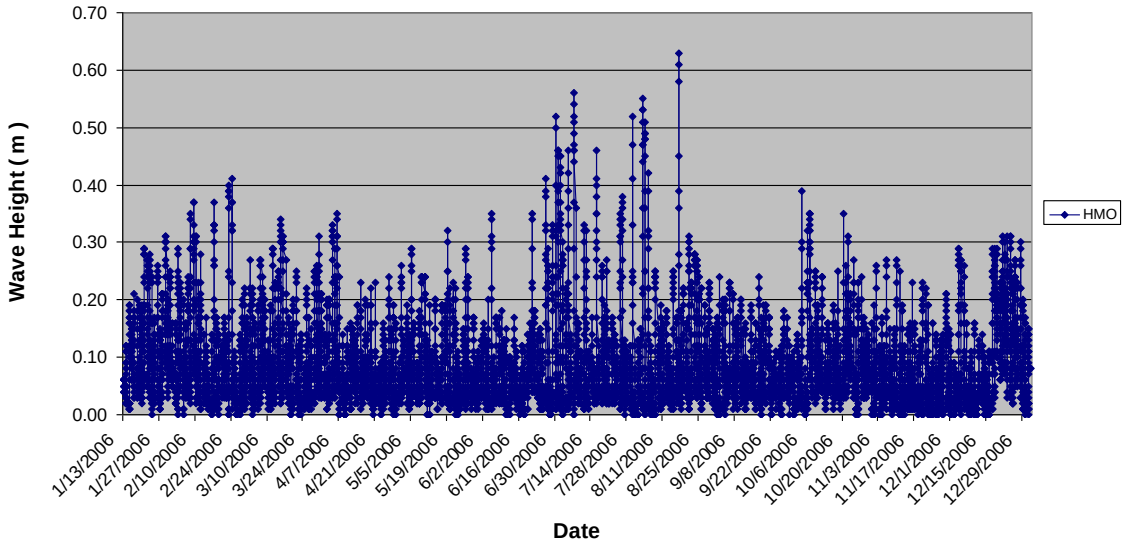

Figure 16 : Offshore waves height for year 2006

Figures 13 to 16 show the graphs for the hindcasted wave heights for the four years from 2003 to 2006, respectively. In general, wave heights are less than 0.8 meter and rarely higher than 1.0 meter. The average wave height for this data series is 0.1 meter only. However, the highest waves occurred on the 4th of October 2003 with a predicted 1.2 meter height approaching from 260^{o} direction (true North).

To evaluate nearshore waves and sediment transport for the highest incident wave height cases, waves from 280^{o} direction was used instead of 260^{o}. Since the study area is located northeast of the island, waves from 260^{o} direction are blocked by the west side of the Island and they will not reach the area offshore of the study site. The highest height for waves from 260^{o} direction was 1.02 meter with a 3.3 second wave period. These values were used as input parameters for the first scenario employed in the wave transformation simulation with EBED.

4.2 Nearshore waves

When wind waves generated in deep water enter shallow water, the wave characteristics will change due to interaction between the waves and the bottom. Wave transformation refers to changes in wave characteristics during propagation from deep to shallow water. According to Mase et al. (2005) sea waves propagating from offshore to the beach change their height, length, and direction according to the particular bathymetry and the presence of currents and structures. The primary processes affecting wave transformation are refraction, diffraction, reflection, and wave breaking.

Wave refraction is a process that affects the distribution of wave energy. It depends on the relation of water depth to wavelength (SPM, 1984). Wave refraction results from a change in wave speed due to local depth changes. In deeper water, waves are moving faster than in shallow water. This will lead to variation in wave speed along the crest of a wave moving at an angle to the underwater contours. The variation in wave speed along the crest of a wave causes the wave crest to bend to aligns with the contours. Wave refraction can result in convergence or divergence of the wave energy causing changes in wave height and wave direction in the nearshore (SPM, 1984).

Diffraction of water waves is a phenomenon in which energy is transferred laterally along a wave crest (SPM, 1984). Energy will spread into the shadow zone when waves encounter an obstacle, such as a breakwater, headland, or an island. Changes in the height along the wave crest for the same wave makes the wave turn into the sheltered region. As a result, wave height and direction will change.

When waves impact a reflective surface, the wave direction will change. This is known as wave reflection, which may be observed when waves hit a breakwater. Wave reflection may also occur when waves encounter the shoreline and can be seen when headlands or bays are present along the shoreline.

There is limiting wave steepness, which is a function of the relative water depth over wave length and the beach slope, determines the maximum wave height that may occur as the waves move from deep water into shoaling water. A wave of given deepwater characteristics will move toward the shore until the water becomes shallow enough to initiate breaking. The water depth when incipient breaking occurs is called the breaking depth, h_b (SPM, 1984).

Linear wave theory was used to determine breaking wave conditions and the general characteristics of waves. Waves start to break when a certain ratio is reached between the wave height and the water depth. This ratio is known as the breaker depth index, γ_b (the index *b* is used to indicate conditions at breaking),

$$\gamma_b = \frac{H_b}{h_b} \qquad (4.21)$$

where H_b is the wave height and h_b is depth at breaking. The breaker depth index, γ_b depends on the beach slope, m and on the incident wave steepness. For this case a value of γ_b is 0.78, which is typical for depth-limited breaking.

The wave properties at breaking are obtained by solving the wave energy flux conservation equation and Snell's Law describing wave refraction. For the case of waves from deep water towards a straight shorelines with parallel offshore bottom contours, the change of wave direction may be approximated by (Snell's Law),

$$\frac{\sin\theta_o}{C_o} = \frac{\sin\theta_b}{C_b} \qquad (4.22)$$

where θ_o is the angle between the deepwater wave crest and the shoreline, θ_b is the angle between the wave crest and the shoreline at breaking, C_o is offshore wave speed, and C_b is wave speed at breaking.

The expression for the wave energy flux per unit width F is given by:

$$F = EC_g \cos\theta \qquad (4.23)$$

In equation (4.23), E is the energy density, C_g is the group speed for the approaching waves, and θ is the angle between the incoming wave crests and the shoreline. The energy density per unit area given in equation (4.23) is defined by, where ρ is the density of water and H is wave height:

$$E = \frac{1}{8}\rho g H^2 \qquad (4.24)$$

For waves in deep water, the phase speed, C, and group speed, C_g, of the waves, respectively, are given by:

$$C_o = \sqrt{\frac{gL_o}{2\pi}} \qquad (4.25)$$

$$C_{g,o} = \frac{1}{2}C_o \qquad (4.26)$$

The phase and group speed for breaking waves are approximately equal for shallow water condition:

$$C_b = C_{g,b} = \sqrt{gh_b} \qquad (4.27)$$

From equation (4.23) and (4.24), the wave energy flux can be express as below:

$$F = \frac{1}{8}\rho g H^2 C_g \cos\theta \qquad (4.28)$$

The offshore wave energy flux can be set equal to the wave energy flux at breaking by assuming that the energy loss due to bottom friction for waves approaching the beach is negligible until incipient breaking condition is reached, yielding the following equation:

$$H_o^2 C_{go} \cos\theta_o = H_b^2 C_{gb} \cos\theta_b \qquad (4.29)$$

Combining this equation with Snell's Law, and assuming small angles at breaking, the water depth at the break point, h_b can be calculated from the following equation:

$$\frac{h_b}{L_o} = \left(\left(\frac{H_o}{L_o} \right)^2 \frac{\cos\theta_o}{\gamma_b^2 2\sqrt{2\pi}} \right)^{2/5} \qquad (4.30)$$

Equation (4.30) was employed to compute the conditions at breaking, from which the sediment transport could be calculated. In the project area the output from the EBED model was used to calculate wave conditions in the nearshore prior to breaking that subsequently were used as to input equation (4.30). Since deepwater wave conditions are needed in this equation, the calculated nearshore wave characteristics by EBED Model were used to determine the wave characteristics in deep water by backing out the waves. Once the deep water wave conditions were known, equation (4.30) was used to calculate the wave parameters at breaking.

To study nearshore waves along the coastline from Tanjung Tokong until Georgetown before and after the reclamation project, four scenarios with different approaching wave angles were investigated. Thus, there were eight cases for the nearshore wave simulations that will be discussed in chapter 6. A summary of the incident wave parameters are given in Table 3.

Table 3 : Wave parameters employed for different scenarios and cases

Scenario	Wave height (m)	Incoming Wave Direction (^{o})	Time Period (s)	Case
1	1.05	280	3.33	Case 1 (before)
				Case 2 (after)
2	0.73	320	3.10	Case 3 (before)
				Case 4 (after)
3	0.62	0	2.79	Case 5 (before)
				Case 6 (after)
4	0.76	40	3.38	Case 7 (before)
				Case 8 (after)

All cases simulated were done at mean sea water level which is +1.6 mean above reference sea level (masl) based on British Admiralty Sea Charts. Reference sea level in British Admiralty Sea Charts referred to Lowest Astronomical Tide (+0.0 meter). The first scenario represents the incoming waves with the largest height based on the wave hindcasting. Scenario 2 represents the largest fetch length for the study area with the largest height for that direction. Wave directions from north (0^{o}) and 40^{o} were used in the third and fourth scenarios, respectively, to see the effects of these different directions. The wave height used in all scenarios was the largest value obtained from the hindcasted wave time series for each direction.

4.3 EBED Model

Wave transformation models are used to assess the wave conditions in coastal and estuarine areas, for a given offshore wave climate, bottom topography, water level, current field, and maritime structures (Mase, 2001). There is a range of wave transformation models have been developed to predict nearshore wave conditions. However, there is no model that is sufficiently general to address all problems related to nearshore wave transformation. Each model has its own strengths and weaknesses. Thus, in order to choose the most suitable wave transformation model, one should consider the advantages and the limitation of a particular model.

Since the main objective of this study was to evaluate wave transformation, sediment transport, and coastal evolution due to coastal reclamation activities on the Tanjung Tokong coastline, the EBED Model was chosen to predict nearshore wave conditions.

The EBED model is a prediction model for multi-directional random wave transformation, based on an energy balance equation and a parabolic approximation wave equation. This model was developed by Hajime Mase from Disaster Prevention Research Institute, Kyoto University, Japan. The model is based on an energy balance equation with an energy dissipation term and a newly formulated diffraction term. EBED takes into account all major nearshore wave transformation processes of importance for the

present study such as shoaling, refraction, diffraction, and dissipation effects. Wave reflection is not included, but this process is negligible for the present application.

The input parameters to EBED are wave height, wave period, and wave direction from true north at the offshore model boundary. In EBED programme, several different boundary conditions may be specified such as an open sea boundary, a reflecting wall boundary, and a dissipative beach boundary (Mase, 2001). In the estimate of the energy dissipation due to breaking, a Rayleigh distribution is assumed and employed to calculate the necessary wave parameters. The energy dissipation coefficient, γ_b, is formulated by using the Goda breaking criterion.

Wave diffraction effects are introduced into the spectral wave energy balance equation through the wave propagation velocities. The grid system defines the location where the spectral density and velocities are calculated.

5. Nearshore Sediment transport

The nearshore wave climate can be determined based on the statistical distributions of the wave characteristics along the shoreline. Important wave characteristics affecting sediment transport near the beach are height, period, and direction of breaking waves (SPM 1984).

Waves affect the sediment transport in the littoral zone in two ways, by initiating sediment movement and by driving a mean longshore current that transports the sediment once it has been mobilized by the waves (SPM 1984). Breaker height is significant in determining the quantity of sand placed in motion and breaker direction is a major factor in determining the magnitude of the longshore transport and its direction.

Higher waves will break further from the shore, widening the surf zone and also setting more sand in motion. Changes in wave period or height cause sand to move onshore or offshore. The angle between the crest of the breaking wave and the shoreline determines the direction of the longshore component of water motion in the surf zone and, usually, the longshore transport direction (SPM 1984).

The resulting movement of shore sediment in the littoral zone is called littoral transport, where the littoral zone extends from the shoreline to just beyond most of seaward breakers. The sediment that moves along the coast is referred to longshore sediment transport, and the corresponding rate Q is known as the longshore transport rate (SPM 1984). Movement perpendicular to the coast is referred to as the cross-shore sediment transport, but it will not be discussed here since it is of less significance for the present study.

Calculated wave conditions at the break point can be used to predict longshore sediment transport rate through the Energy Flux method (SPM 1984). This method assumes that the longshore transport rate, Q, depends on the longshore component of the wave energy flux in the surf zone.

Thus, the expression for the total longshore sediment transport rate Q is given by,

$$Q = \frac{K}{g(\rho_s - \rho)(1 - a)} P_{ls} \qquad (5.1)$$

where K is the dimensionless coefficient, P_{ls} is the longshore energy flux factor, ρ_s is the sediment density, ρ is the water density, and a is the porosity. Assuming that the longshore transport rate depends on the longshore component of the wave energy flux in the surf zone based on the significant wave height, a value of 0.39 is appropriate for K. In the present study, a value of 2650 kg/m^3 was employed for the sediment density and 0.4 for the porosity.

The longshore energy flux is expressed as,

$$P_{ls} = \frac{\rho g}{16}\left(H^2 C_g \sin\left(\theta\right)\right)_b \qquad (5.2)$$

where H_b is the breaking wave height, C_{gb} is the breaking wave group speed, and θ_b is the angle between the breaking waves and the shoreline.

The longshore transport takes place parallel to the shoreline and there are two possible directions of motion, right to left and vice versa, relative to an observer standing on the shore looking out to sea. The quantity Q_{rt} denotes the sediment transport rate in the right direction and Q_{lt} is the sediment transport rate in the left direction. The sum of Q_{rt} and Q_{lt} is called the gross longshore transport rate, Q_g. Furthermore, the difference between the amount of Q_{rt} and Q_{lt} is known as net longshore transport rate, Q_n. The definition of these quantities and some others are:

$$Q_g = Q_{rt} + Q_{lt} \qquad (5.3)$$

$$Q_n = Q_{rt} - Q_{lt} \qquad (5.4)$$

$$\gamma = \frac{Q_{lt}}{Q_{rt}} \qquad (5.5)$$

$$Q_g = Q_n \frac{\left(+\gamma\right)}{\left(-\gamma\right)} \qquad (5.6)$$

In assessing the sediment transport behaviour for the study area, the long-term transport rate patterns for the northern area was computed as well as the transport pattern in the land reclamation area before and after the fill. For the long-term transport the hindcasted wave time series was used as input, whereas for the study of the fill effects selected scenarios were employed, as previously discussed.

By knowing the nearshore sediment transport rate, the shoreline response can be predicted implying either accumulation or erosion depending to the alongshore sediment transport gradients.

5.1 Regional sediment transport pattern

The available hindcasted four-year wave time series was used to derive the regional longshore sediment transport pattern along the northern coast. Five shoreline stretches along the Tanjung Bungah coastline along the north part of the island were identified to compute the sediment transport rate as shown in figure 17.

The shoreline orientation (angle) to the horizontal for each of the identified shoreline stretches are presented in table 4. These orientations were used to calculate the angle between the incoming waves and the shoreline.

Breaking wave characteristics were obtained from the offshore hindcasted wave data series for the four years. After the breaking wave characteristics were available, sediment transport rate, Q, were calculated using equations 5.1 and 5.2 for each wave in the time series. The gross longshore transport rate, Q_g, and net longshore transport rate, Q_n, were calculated to obtain the regional sediment transport pattern as an average over the four years studied.

Table 4 : Shoreline orientation from the horizontal used to calculate the angle between incoming waves and shoreline

Shoreline stretch	Shoreline orientation from horizontal
L1	3^o
L2	13^o
L3	5^o
L4	9^o
L5	5^o

Table 4 summarizes the sediment transport rates Q_{lt} and Q_{rt} as well as the gross longshore transport rate, Q_g and the net longshore transport rate, Q_n for the five selected shoreline stretches. The net longshore transport rates for location L1 and L5 were found to be positive implying that the net sediment movement is towards the right along the shore. In contrast, the negative values on net longshore transport rate, Q_n, for L2, L3, and L4 indicate alongshore sediment movement towards the left. Even though Q_n at Location L5 is rather small value, there is still available sediment from north part of the island that will move towards the project area.

Table 5 : Calculated gross longshore transport rate Q_g and net longshore transport rate Q_n for obtaining regional sediment transport pattern

Shoreline stretch	**Q_{rt} (m^3/y)**	**Q_{lt} (m^3/y)**	**Q_g (m^3/y)**	**Q_n (m^3/y)**
L1	12,900	11,500	24,400	1,400
L2	11,800	17,000	28,800	-5,200
L3	12,800	13,000	25,800	-200
L4	14,000	15,600	29,600	-1,600
L5	14,400	10,800	25,200	3,600

Figure 17 : Five selected shoreline stretches to calculate regional sediment transport pattern at northern Penang Island

From Figure 17, in general, net sediment transport for these locations vary with sediment moving towards right or left along the shore. Net sediment transport at L2, L3 and L4 is towards left along the shore, whereas net sediment transport at L1 and L2 is towards right along the shore. These patterns were compared with observed sediment features observed from Google Earth photos.

Figure 18 : Google earth photo at location L1

Figure 18 shows the Google Earth photo at location L1 with two rivers which are affected by the direction of sediment transport. From Figure 17 net sediment transport at location L1 is towards right with a sediment rate of 1,600 m^3/year, and net sediment transport at L2 is in opposite direction with a larger amount of sediment rate 5,200 m^3/year. These calculations are seem to agreed with Figure 18, where the unprotected rivers A and B had affected by the directions of the sediment transport from left and right, respectively.

Figure 19 : Google earth photo at location L2

Figure 19 shows a close-up of the beach at location L2 where the net sediment transport is 5,200 m^3/year towards left along the shore. Long beach at Tanjung Bungah beach seems not to be affected by sediment transport unless at outlet B, where the outlet is diverted towards the left due to the strong sediment transport rate at location L2.

Figure 20 : Google earth photo at location L3

Figure 20 shows location L3 from a Google Earth photo. In the small bay, there was a tombolo bend towards the left direction. This indicates that sediment moves toward left and this agrees with the calculated net sediment transport rate as shown in figure 17, where the calculated net sediment transport was 200 m^3/year towards the left side along the shore.

Figure 21 : Google Earth photo at location L4

Figure 21 displays a Google Earth photo at location L4, where L4 is situated in a bay. From the figure it is clearly seen that a stable sandy bay is situated between the structure and the rock revetment on the left side of the photo. A long sandy beach can be seen on the right side of the photo. Even though the calculated net sediment direction indicated transport towards the left along the shore, it can not be clearly seen in figure 21 by any indication in the shoreline pattern. However, the stable sandy bay may indicate that the bay reached equilibrium with the sediment transport in the stable area, which then should mainly come from the left in agreement with the calculations.

Figure 22 : Google Earth photo at location L5

Figure 22 shows the Google Earth photo for location L5 at Tanjung Tokong beach. From the photo, a long beach and a small outlet C on the left side of the photo. This small outlet C has a tendency to be diverted to the right of the direction. Calculated net sediment transport shows that the sediment moves towards the right along the shore with 3,600 m^3/year. Even though the end of this beach is a rocky headland, sediment might move towards the right after the headland due to strong incoming waves from northwest and diffraction effect. This will indicate that there is available sediment that will move towards the study area, which is located east the headland.

5.2 Local sediment transport pattern

The local sediment transport pattern in the area of the land reclamation before and after the fill was determined by, (1) running the EBED model, (2) using the output from EBED to determine the conditions at breaking for selected shoreline stretches, and (3) calculating the longshore transport rate for these stretches. Three shoreline stretches, A, B and C as shown in Figure 23 were selected to calculate the longshore sediment transport rate. The location of the stretches were selected to include areas were maximum effect of the fill was expected with respect to the different incoming wave directions.

The local sediment transport pattern before and after land reclamation was determined for the different stretches and the chosen wave input scenarios. Four scenarios involving different approaching wave angles were employed to determine the local sediment transport pattern before and after reclamation project at each location (A, B and C). Breaking wave characteristics at locations A, B, and C were calculated employing equations (4.21) – (4.30), and based on these calculations the longshore sediment transport rates were obtained. The results concerning the local sediment transport pattern before and after the land reclamation will be discussed in the next chapter.

Figure 23 : Shoreline stretches at locations A, B and C used to study local sediment transport pattern before and after the land reclamation

6. Effects of Land Reclamation

With the overall aim to study the effects of the land reclamation on waves and sediment transport, all simulations were done for conditions before and after the fill. Nearshore wave simulations were carried out using the EBED model, as previously discussed. The breaking wave conditions and the alongshore sediment transport were calculated based on the EBED simulation results.

6.1 Nearshore waves

Nearshore wave simulation was done for eight cases including conditions before and after the project. Simulations were performed at mean sea water level. The results are summarized in the following.

Table 6: Nearshore wave characteristics for different scenarios and before and after the land reclamation

Scenario 1 : H=1.05m Wave direction=280^o T=3.33s						
Cases	**Location**	**H_in (m)**	**Wave Direction (^{o})**	**T_in (s)**	**h_in (m)**	**θ_in (degree)**
Case 1 before project	A	0.23	12	3.4	1.3	18
	B	0.19	4.6	2.6	1.8	30.4
	C	0.26	347	2.7	4.3	13
Case 2 after project	A	0.17	24.5	3.8	1.2	5.5
	B	0.18	8.4	2.7	1.8	26.6
	C	0.25	346.5	2.7	4.3	13.5
Scenario 2 : H=0.73m Wave direction=320^o T=3.1s						
Cases	**Location**	**H_in (m)**	**Wave Direction (^{o})**	**T_in (s)**	**h_in (m)**	**θ_in (degree)**
Case 3 Before project	A	0.33	15	3.1	1.3	15
	B	0.27	12.4	2.6	1.8	22.5
	C	0.39	351.6	2.8	4.3	8.4
Case 4 After project	A	0.26	25	3.2	1.2	5
	B	0.27	13.5	2.7	1.8	21.5
	C	0.39	352	2.8	4.3	8

Scenario 3 : H=0.62m Wave direction=0^{o} T=2.79s						
Cases	**Location**	**H_in (m)**	**Wave Direction (^{o})**	**T_in (s)**	**h_in (m)**	**θ_in (degree)**
Case 5 Before project	A	0.33	24.4	2.8	1.3	5.6
	B	0.27	24.3	2.6	1.8	10.7
	C	0.39	7.9	2.7	4.3	7.9
Case 6 After project	A	0.41	31.3	2.8	1.2	1.3
	B	0.43	24.4	2.6	1.8	10.6
	C	0.55	8.1	2.8	4.3	8.1
Scenario 4 : H=0.76m Wave direction=40^{o} T=3.38s						
Cases	**Location**	**H_in (m)**	**Wave Direction (^{o})**	**T_in (s)**	**h_in (m)**	**θ_in (degree)**
Case 7 Before project	A	0.7	51	3.6	1.3	21
	B	0.57	51	3.4	1.8	16
	C	0.73	41	3.3	4.3	41
Case 8 After project	A	0.65	53.2	3.6	1.2	23.2
	B	0.67	50.8	3.4	1.8	15.8
	C	0.73	41.2	3.3	4.3	41.2

Table 6 shows the nearshore wave characteristics for the four scenarios employed before and after the fill, encompassing in total eight cases. Wave height, wave direction, and wave angle will be discussed for each scenario and case.

Figures 24 to 31 show nearshore wave directions in the area and the representative values at locations A, B, and C for all eight cases, whereas Figure 32 to 35 presents comparisons of the wave heights at locations A, B and C for each scenario before and after the fill.

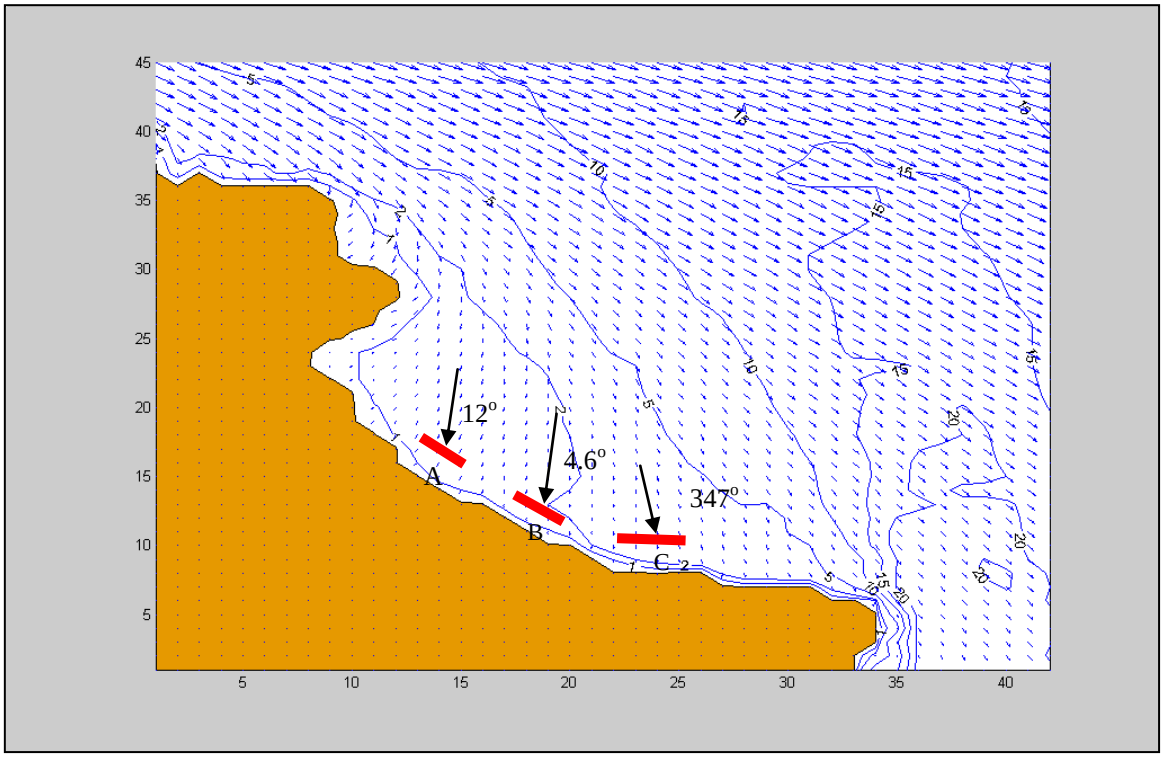

Figure 24 : Case 1 before project with wave direction 280°, wave height 1.06 m, and wave period 3.3 s

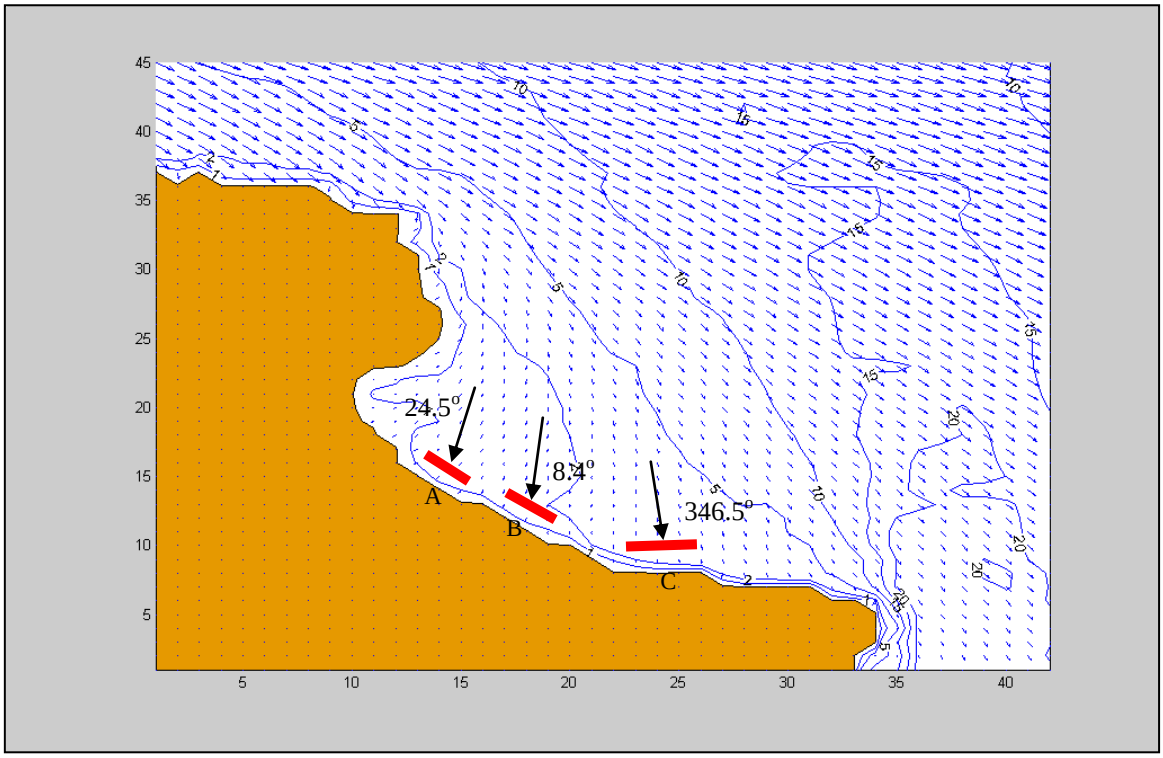

Figure 25 : Case 2 after project with wave direction 280°, wave height 1.06 m, and wave period 3.3 s

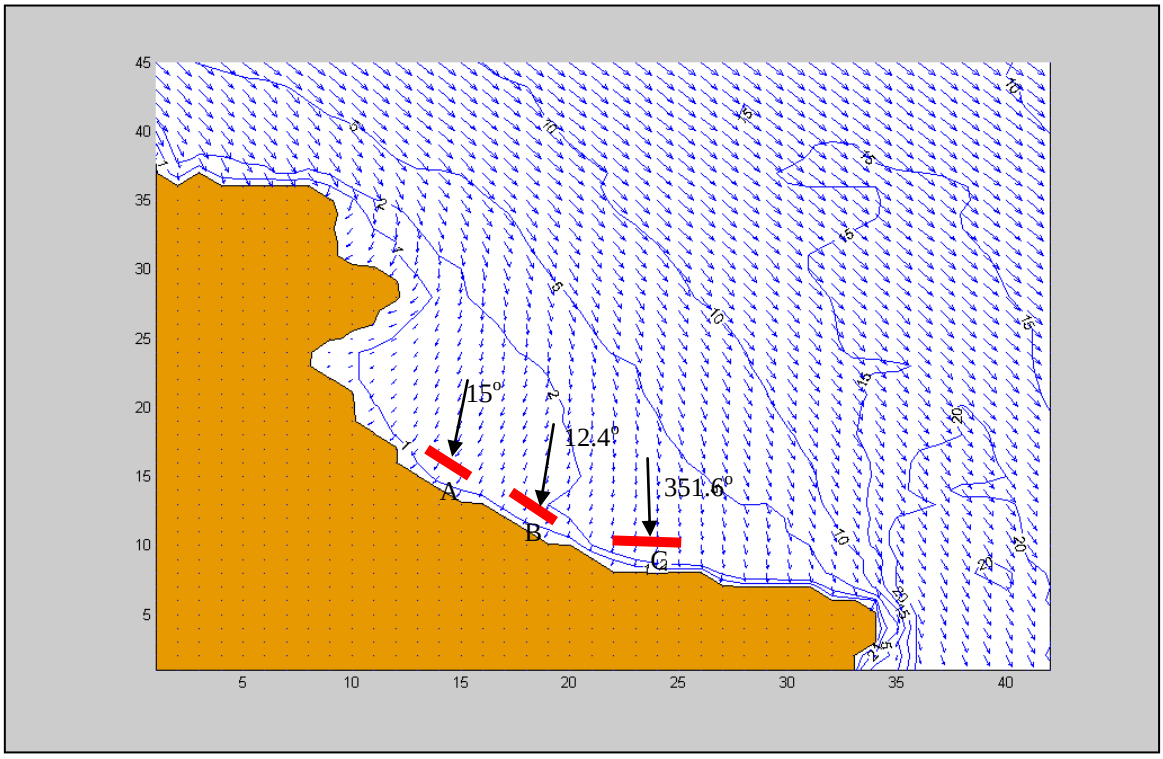

Figure 26 : Case 3 after project with wave direction 320°, wave height 0.73 m, and wave period 3.1 s

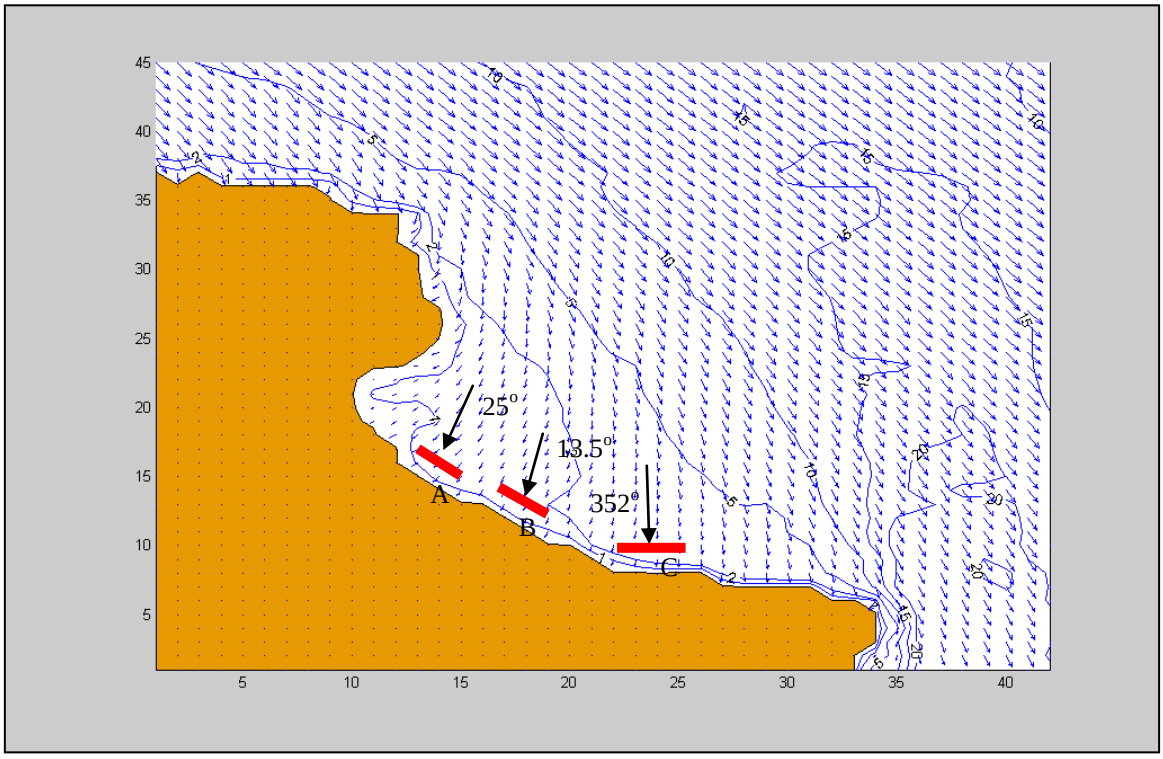

Figure 27 : Case 4 after project with wave direction 320°, wave height 0.73 m, and wave period 3.1 s

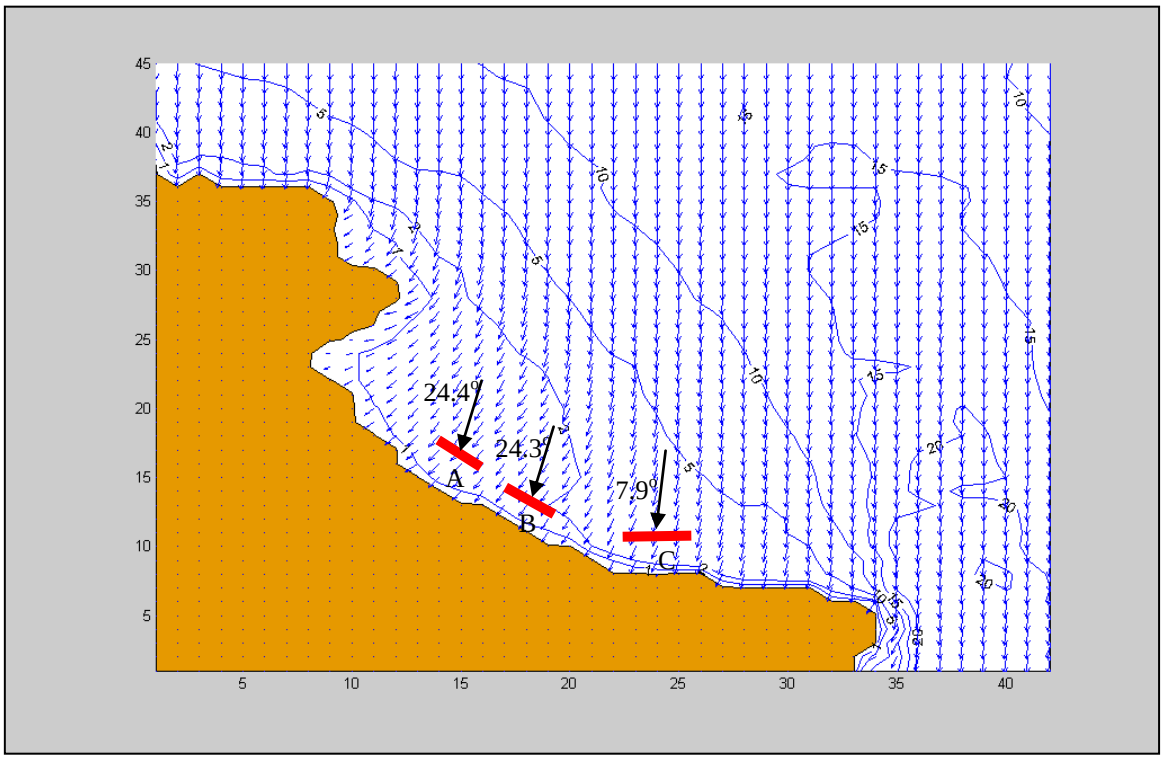

Figure 28 : Case 5 after project with wave direction 0°, wave height 0.62 m, and wave period 2.79 s

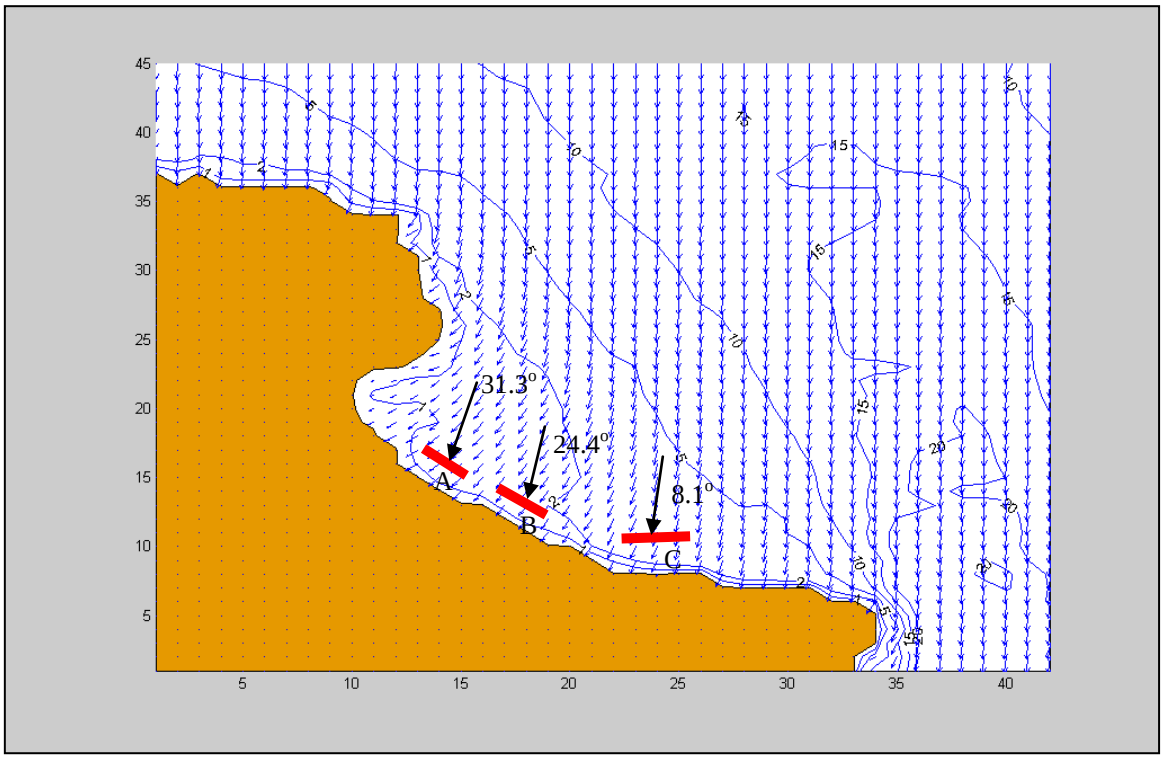

Figure 29 : Case 6 after project with wave direction 0°, wave height 0.62 m, and wave period 2.79 s

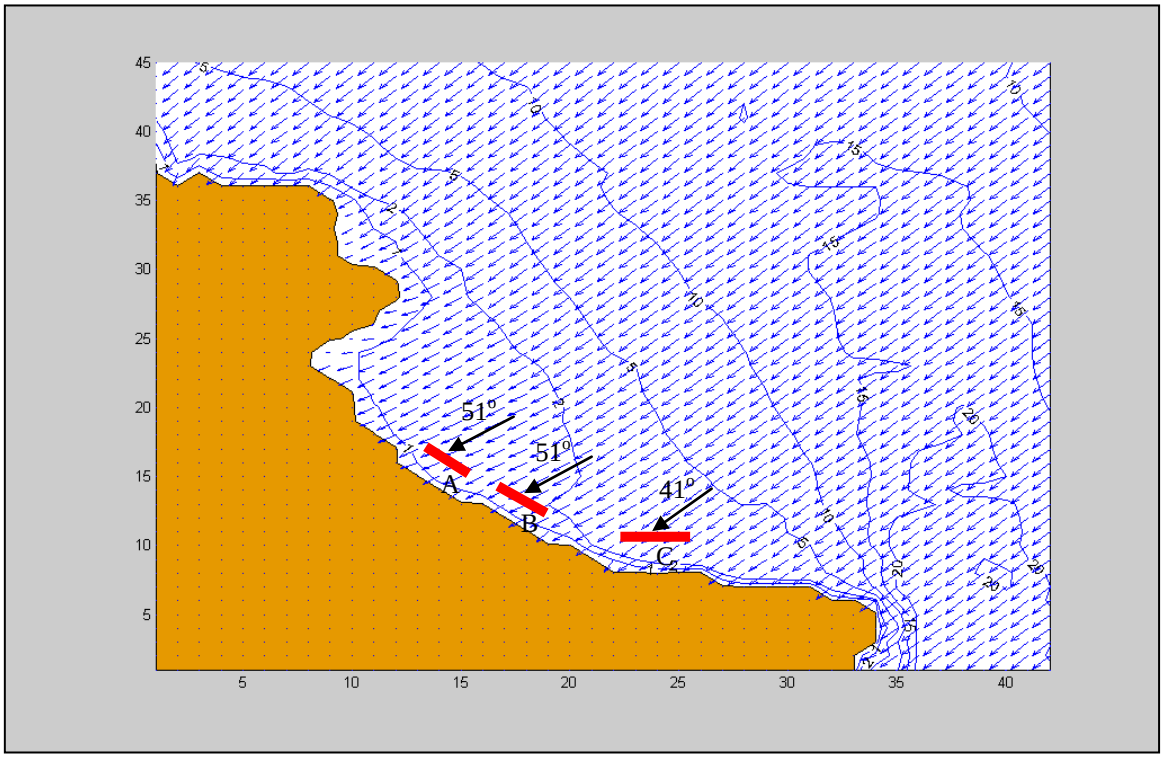

Figure 30 : Case 7 after project with wave direction 40°, wave height 0.76 m, and wave period 3.38 s

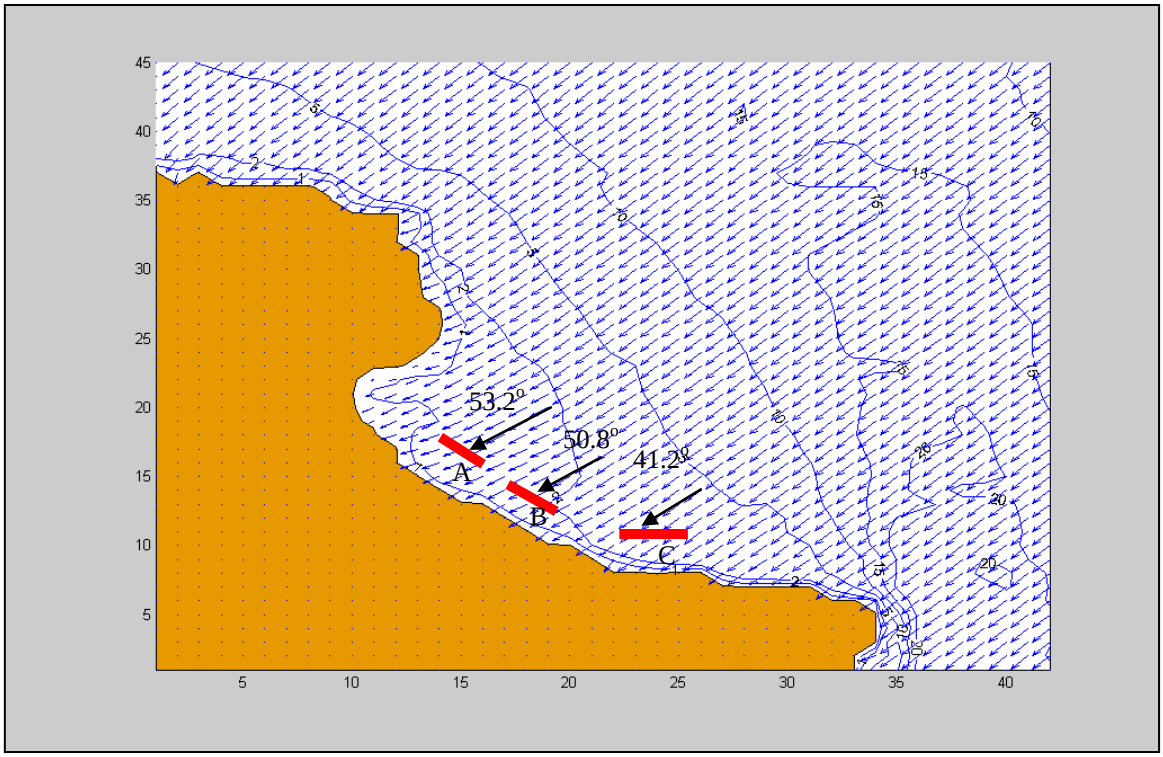

Figure 31 : Case 8 after project with wave direction 40°, wave height 0.76 m, and wave period 3.38 s

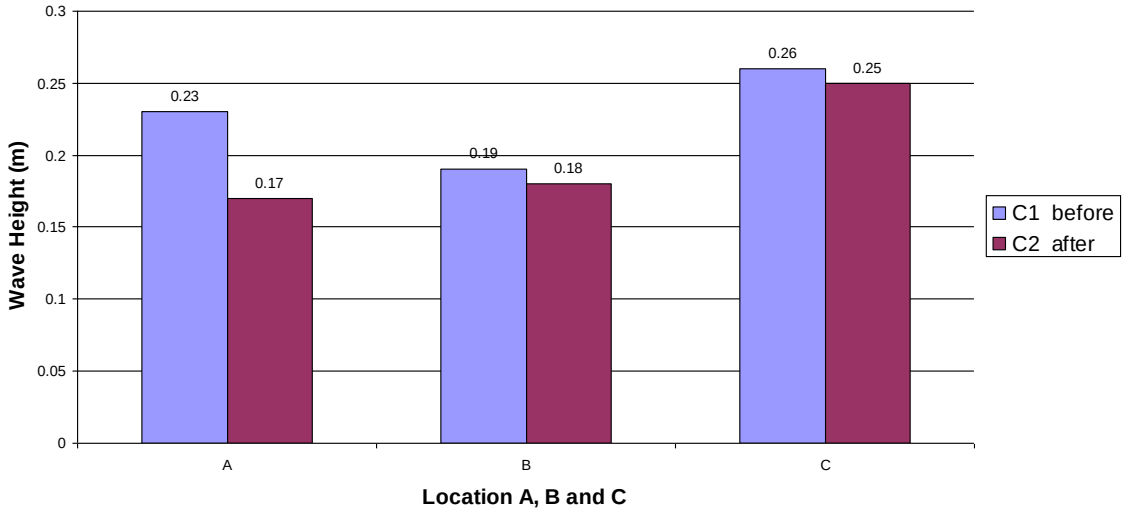

Figure 32 : Comparison of nearshore wave heights before and after project conditions at location A, B, and C for 280^{o} incoming wave direction

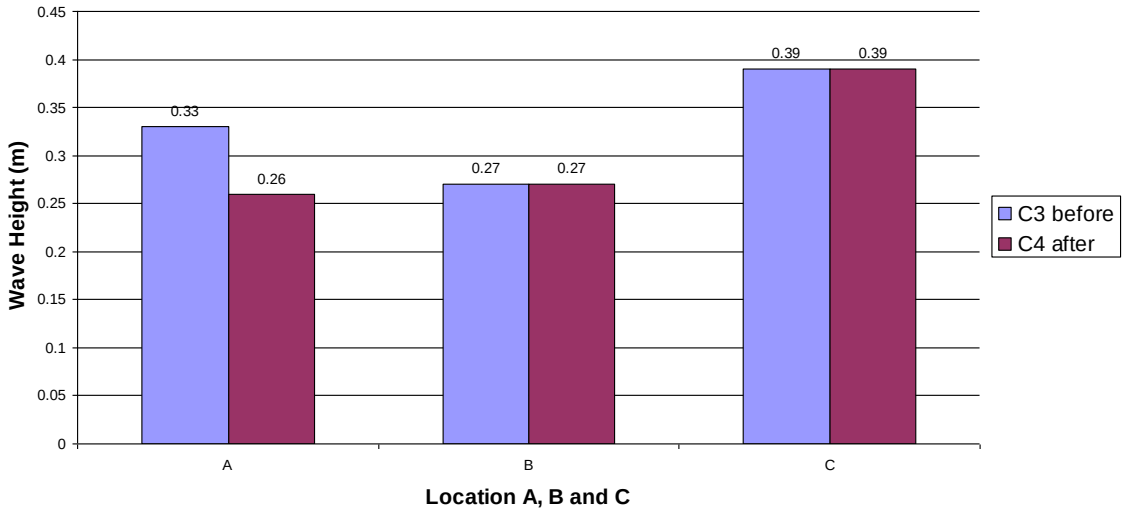

Figure 33 : Comparison of nearshore wave heights before and after project conditions at location A, B, and C for 320^{o} incoming wave direction

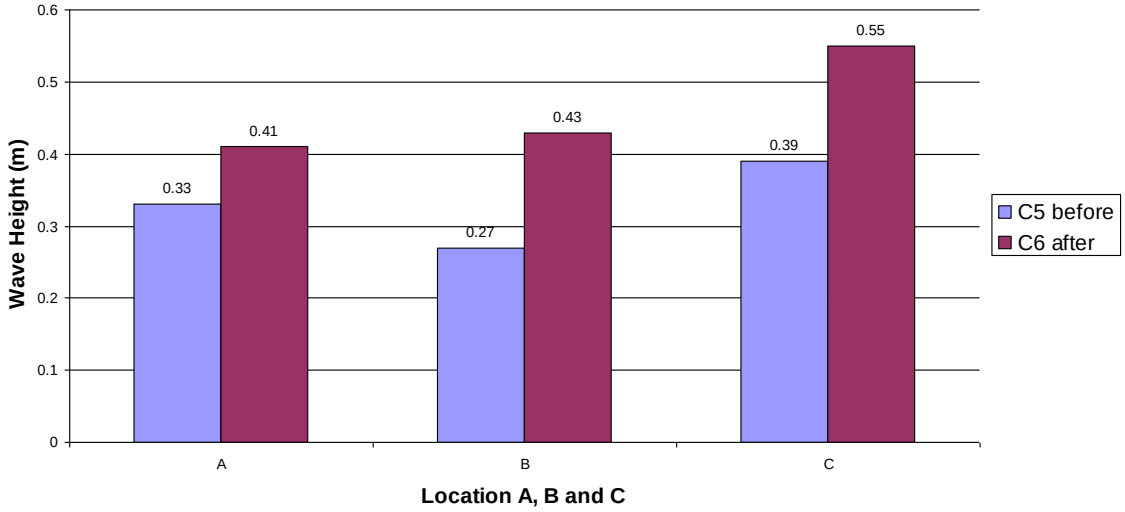

Figure 34 : Comparison of nearshore wave heights before and after project conditions at location A, B, and C for 0^o incoming wave direction

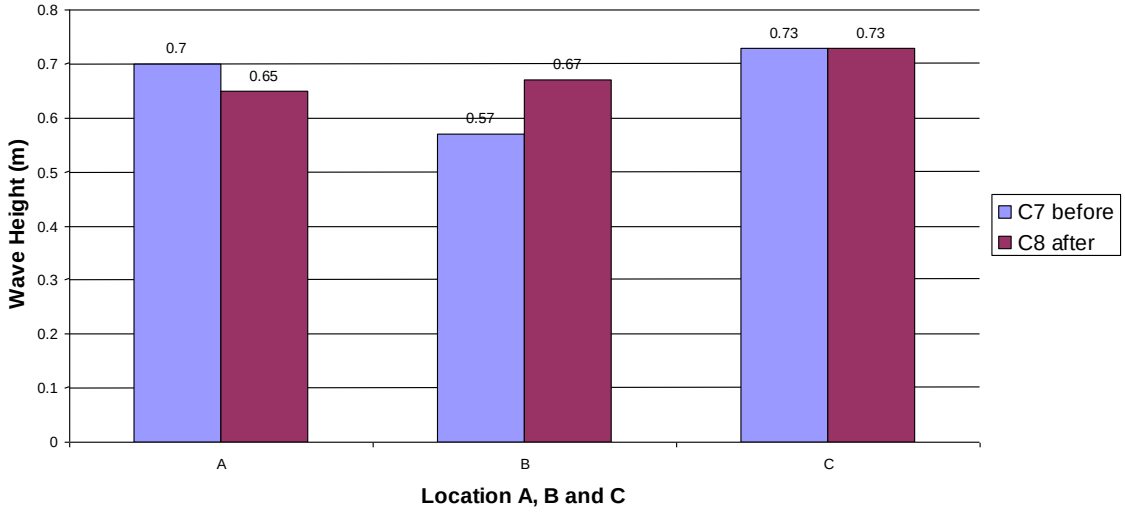

Figure 35 : Comparison of nearshore wave heights before and after project conditions at location A, B, and C for 40^o incoming wave direction

Figures 24 to 31 show the nearshore waves transformation before and after the land reclamation project for each scenario. It clearly shows that the direction of the waves changed after the project. The land reclamation project caused changed wave conditions at the shoreline by enlarging the land area towards the sea, influencing the wave transformation behaviour. The wave transformation is influenced by diffraction, refraction, and shoaling processes. After the land reclamation, especially the diffraction pattern south of the fill is affected.

Nearshore wave transformation for the first scenario with case 1 before project and case 2 after project are shown in figure 24 and 25, respectively. In the first scenario, offshore wave direction was 280^o, significant wave height 1.06m, and wave period was 3.3s. These wave characteristics markedly changed when the waves reached the shallow area at Tanjung Tokong. The nearshore wave direction at location A and B changed from 12^o to 24.5^o and 4.6^o to 8.4^o, correspondingly. However there was not so much difference at location C with 347^o before project and 346.5^o after project. Offshore waves from 280^o direction were diffracted by Tanjung Tokong Headland and they changed direction coming closer to shore. After project, waves diffracted more because of the changes in the shoreline orientation in the project area.

For the second scenario, the offshore wave direction was 320^o, significant wave height 0.73m, and wave period 3.1s. The nearshore wave transformation for before, case 1, and after land reclamation project, case 2, are shown in figures 26 and 27. Nearshore waves were also diffracted by the Tanjung Tokong Headland and the most significant change due to the project was at location A. For the case before project, the nearshore wave direction was 15^o and this angle increased to 25^o after project. However, there were not any significant differences in the nearshore wave direction at location B and C before and after the project. Waves from a 320^o direction were less diffracted compared to waves from 280^o.

Figures 28 and 29 show the results of the EBED simulations for the third scenario with offshore wave conditions: incoming wave direction from north, 0^o, significant wave height 0.62m, and wave period 2.79s. Similar to the previous scenarios, location A experienced the most significant changes in the nearshore wave characteristics. However, in this scenario, shallow water was the most important factor influencing nearshore wave characteristics. At location A, the water depth was shallower than at the other locations, thus, the nearshore waves at location A were more diffracted compared to at locations B and C. The project also influenced the degree of diffraction at location A, where the nearshore wave direction after the project increased to 31.3^o compared to 24.4^o before the project. Locations B and C were not affected by the project because of the distance from the project area with regard to the extent of the shadow zone related to diffraction.

A wave direction of 40^o, significant wave height 0.76m, and wave period 3.38s were used as offshore conditions to simulate the fourth scenario. From figures 30 and 31, it can be seen that the nearshore wave direction did not differ much before the project and after the project. However, nearshore wave directions were slightly affected by diffraction due to the shallow water at locations A and B. Location A was still affected by the project with the nearshore wave direction being 51^o and 53.2^o before and after the project, respectively. There were not significant changes for the nearshore wave directions at locations B and C before and after the project.

In summary, after the project, transformation of the incoming waves from the western direction was more significant compared to incoming waves from the north and east direction. When waves travel to shore, diffraction and shoaling processes play important

roles in wave transformation. Therefore, changes in shoreline alignment and sea bed contours effect the wave transformation.

Overall, there were changes in the nearshore wave heights for each scenario and case. For the first scenario, the incoming waves were from 280^o direction (true north) with wave height 1.06 meter and wave period 3.33 second. A wave height of 1.06 meter represented the highest incident wave height encountered in the project area. As seen in the figure 32, there were changes in nearshore wave height between before and after the project at location A. The wave height decreased after the project with 26% from 0.23 meter to 0.17 meter. However, there was no significant change in wave height at locations B and C. After the project, the nearshore wave directions slightly changed at location A and B. At location A, the nearshore wave direction before and after the project was 12^o and 24.5^o, respectively, as discussed before. At location B, the nearshore wave direction before an after the project were 4.6^o and 8.4^o, respectively. Transformation in wave directions caused changes in the angle between the wave crest and the shoreline, θ. However, there was not significant change in the nearshore wave direction at location C. Also, the wave period at locations A, B, and C were not much different before and after the project.

The second scenario involved incoming waves from 320^o direction with wave height 0.73 meter and wave period 3.1 second. This scenario represents condition for the largest fetch length of the area. From the EBED simulations, location A displayed the most change in nearshore wave height and wave direction due to the land reclamation project. Before the project the nearshore wave height was 0.33 meter and it was reduced by 21% to 0.26 meter after the project. Nearshore wave direction at location A before the project was 15^o and it changed to 25^o after the project. This caused a 67% change in the angle between the wave crest and the shoreline from 15^o to 5^o before and after the project, respectively. Nearshore wave height and direction at locations B and C did not significantly change. Wave periods at all three locations before and after the project were quite similar.

Incoming waves from north (0^o) with wave height 0.62 meter and wave period 2.79 second were the parameters used for the third scenario. The results showed significant increase of nearshore wave heights after land reclamation for locations A, B and C. At location A, before the project, the nearshore wave height was 0.33 meter, however, it increased by 24% to 0.41 meter after the project. The nearshore wave height at location B increased nearly 60% from 0.27 meter to 0.43 meter before and after the project, respectively. In the first and second scenarios, location C did not experience any significant changes, but in the third scenario, the nearshore wave height increased 40% from 0.39 meter before the project to 0.55 meter after the project, respectively. However, only location A experienced change in the nearshore wave direction with 24.4^o before project and 31.3^o after project. Nearshore wave direction at locations B and C did not changed significantly. Similar to the previous scenarios, the wave periods did not change markedly.

For the fourth scenario, incoming wave parameters are: wave direction 40^o, wave height 0.76 meter, and wave period 3.38 second. This incoming wave direction gave relatively higher nearshore wave heights compared to the other three incoming waves previously

discussed. Both before and after the project, nearshore wave heights from this direction were more than 0.5 meter. Location B showed a 17% increase in the nearshore wave height with 0.57 meter before the project and 0.67 meter after the project, respectively. However, in location A the wave height decreased from 0.7 meter before the project to 0.65 meter after the project. Similar to the first and second scenarios, location C was not affected by the project. For the nearshore wave direction, there was a slight change at location A with 51^o before the project and 53.2^o after the project. Locations B and C more or less maintained the directions after the project. Wave period in this scenario also did not change so much, in agreement with the other scenarios.

In summary, nearshore wave characteristics were affected by the land reclamation project. The most affected area was around location A, which is the nearest location to the land reclamation project area. For the highest incident wave height, 1.06 meter from a 280^o direction, the nearshore wave height was reduced significantly after the project due to sheltering, to less than 0.2 meter, especially at Location A. The changes in wave height indicate that the land reclamation project may have marked impact on the coastal evolution in the areas south of the fill.

The reclaimed area changed the shoreline alignment and the bottom topography, which changed the wave transformation from deep water to nearshore. Wave height and direction changed because of refraction, diffraction, and shoaling effects. These effects are the reason why wave characteristics at location A are more affected compared to at locations B and C. These changes in the wave characteristics because of the land reclamation may influence sediment transport, which will be discussed in the next chapter.

6.2 Nearshore sediment transport

After the nearshore wave conditions were determined, the longshore sediment transport were calculated using equations 5.1 to 5.12. The results are shown in following.

Table 7 : Nearshore sediment transport rate at locations A, B, and C for before and after the Land Reclamation Project for each scenario.

Scenario	Case	Location	h_b	H_b	θ_b	Q (m^3/s)	Q (m^3/y)	Direction
Scenario 1	Case 1	A	0.38	0.30	8.46	0.002059	65,000	Q_{rt}
		B	0.34	0.27	11.26	0.002137	67,500	Q_{rt}
		C	0.55	0.43	4.09	0.002602	82,100	Q_{rt}
	Case 2	A	0.30	0.24	2.44	0.000351	11,100	Q_{rt}
		B	0.33	0.26	9.78	0.001717	54,200	Q_{rt}
		C	0.54	0.42	4.17	0.002455	77,500	Q_{rt}
Scenario 2	Case 3	A	0.52	0.40	8.27	0.004373	137,900	Q_{rt}
		B	0.47	0.36	9.91	0.004069	128,400	Q_{rt}
		C	0.77	0.60	3.12	0.004508	142,200	Q_{rt}
	Case 4	A	0.43	0.33	2.64	0.000891	28,200	Q_{rt}
		B	0.47	0.36	9.49	0.003906	123,200	Q_{rt}
		C	0.77	0.60	2.98	0.004297	135,600	Q_{rt}
Scenario 3	Case 5	A	0.53	0.41	3.15	0.001784	56,300	Q_{rt}
		B	0.48	0.37	4.85	0.002138	67,500	Q_{rt}
		C	0.77	0.60	2.94	0.004246	134,000	Q_{lt}
	Case 6	A	0.62	0.48	0.82	0.000699	22,100	Q_{lt}
		B	0.69	0.54	5.79	0.006465	203,900	Q_{rt}
		C	1.01	0.79	3.46	0.009922	312,900	Q_{lt}
Scenario 4	Case 7	A	0.90	0.70	15.22	0.030866	973,400	Q_{lt}
		B	0.85	0.67	9.64	0.017815	561,800	Q_{lt}
		C	1.19	0.93	17.75	0.072365	2,282,200	Q_{lt}
	Case 8	A	0.81	0.63	16.55	0.025499	804,200	Q_{lt}
		B	0.97	0.76	10.17	0.025948	818,300	Q_{lt}
		C	1.19	0.93	17.82	0.072498	2,286,300	Q_{lt}

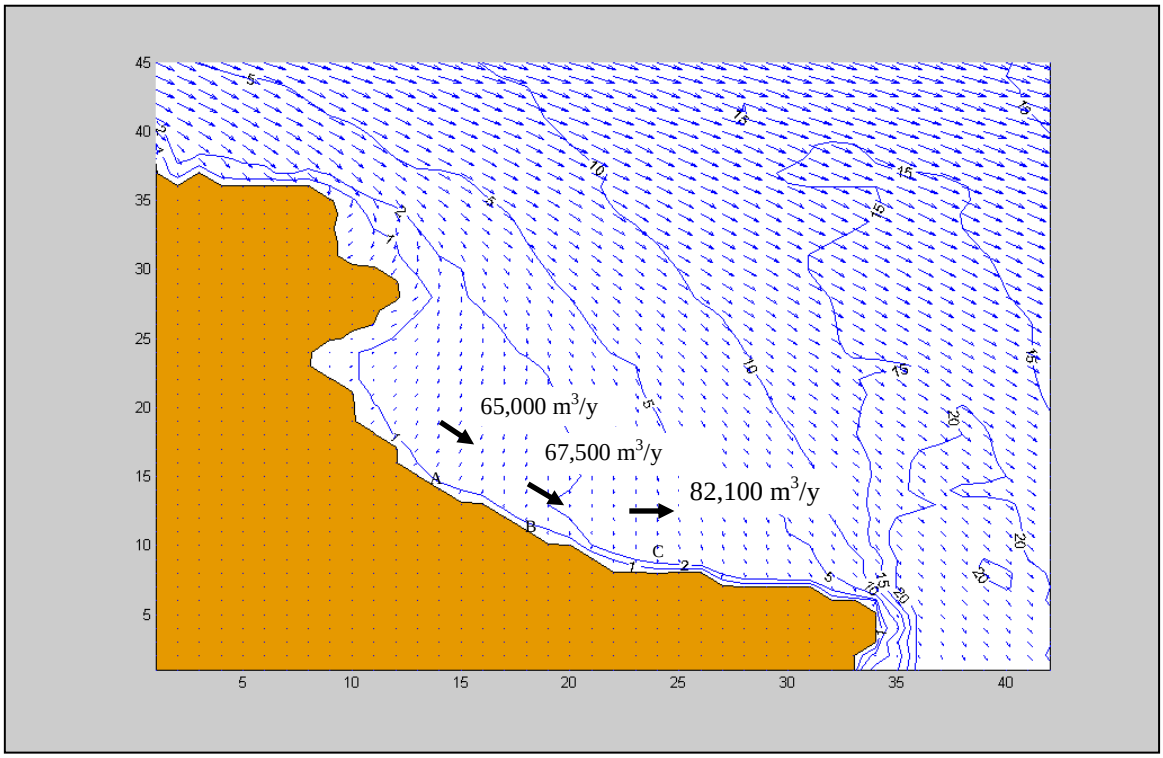

Figure 36 : Local sediment transport rate for case 1 before project with wave direction 280^{o}, wave height 1.06 m, and wave period 3.3 s

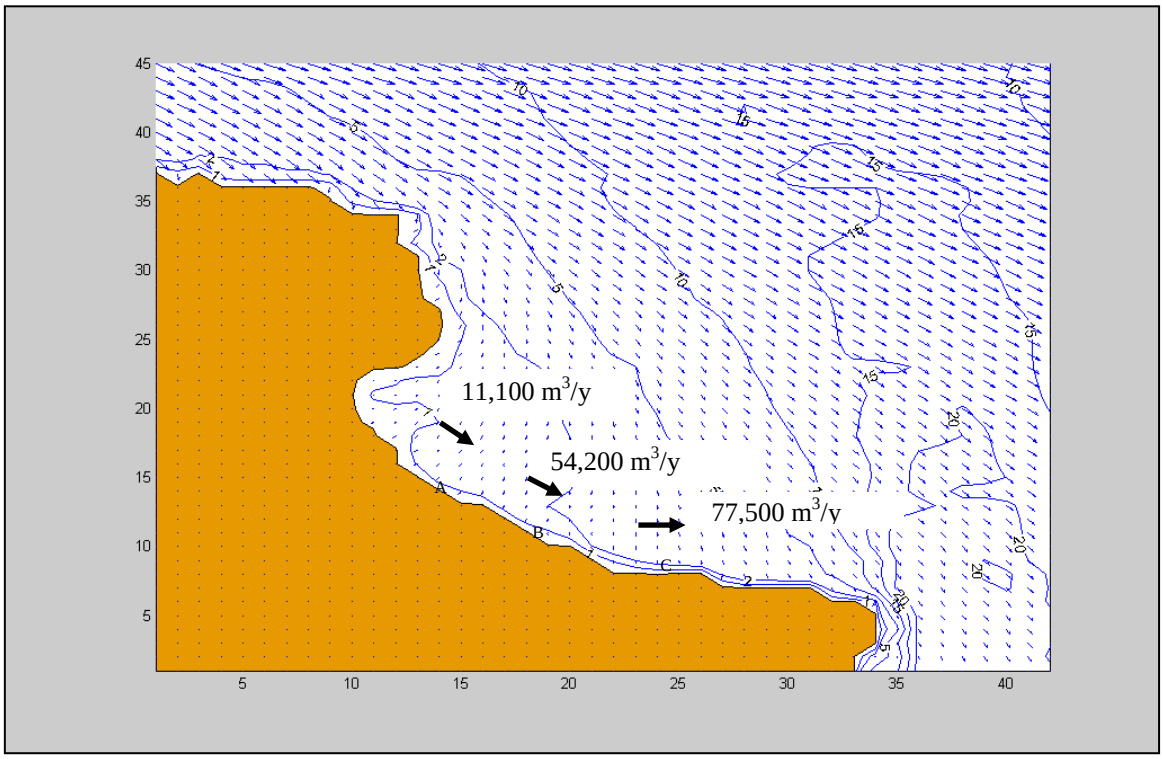

Figure 37 : Local sediment transport rate for case 2 after project with wave direction 280^{o}, wave height 1.06 m, and wave period 3.3 s

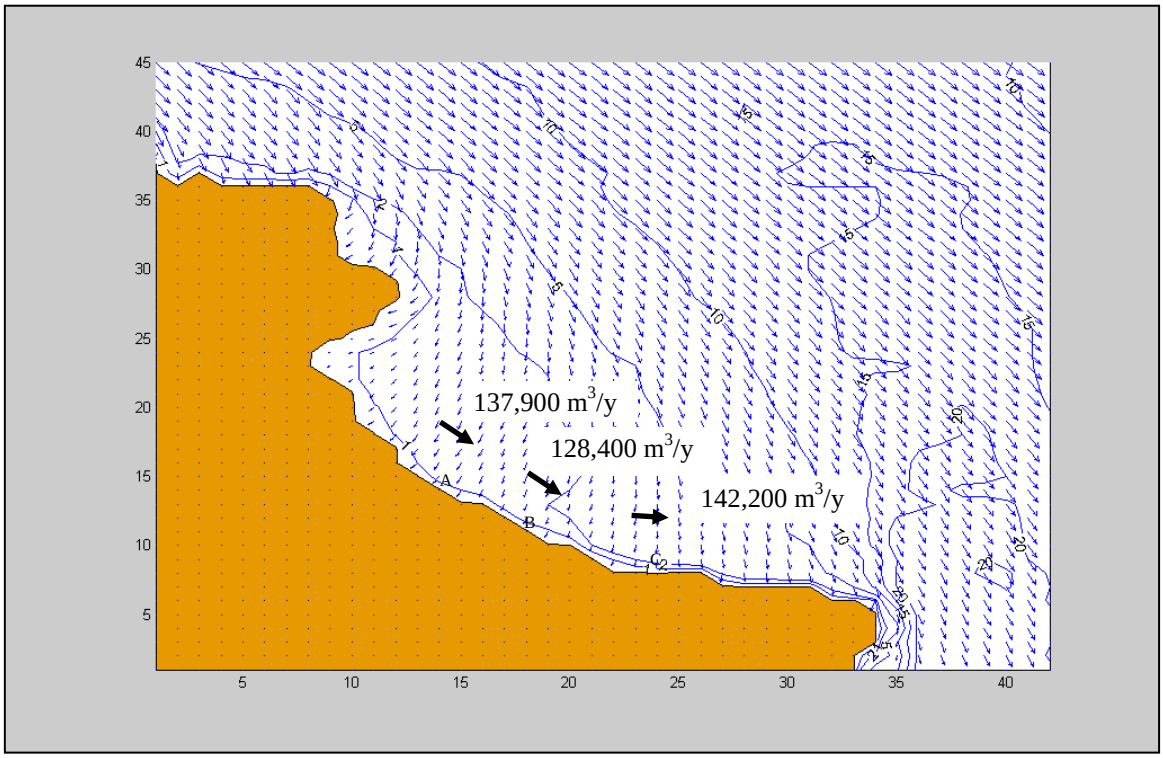

Figure 38 : Local sediment transport rate for case 3 before project with wave direction 320^{o}, wave height 0.73 m, and wave period 3.1 s

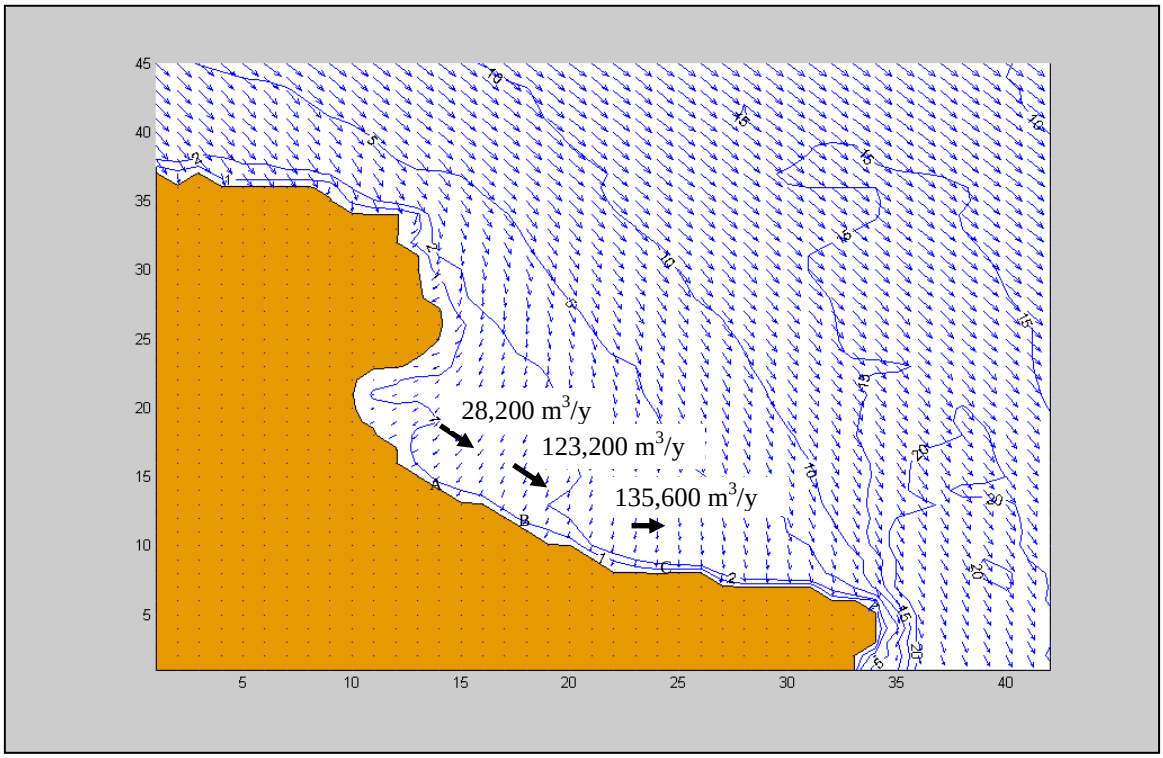

Figure 39 : Local sediment transport rate for case 4 after project with wave direction 320^{o}, wave height 0.73 m, and wave period 3.1 s

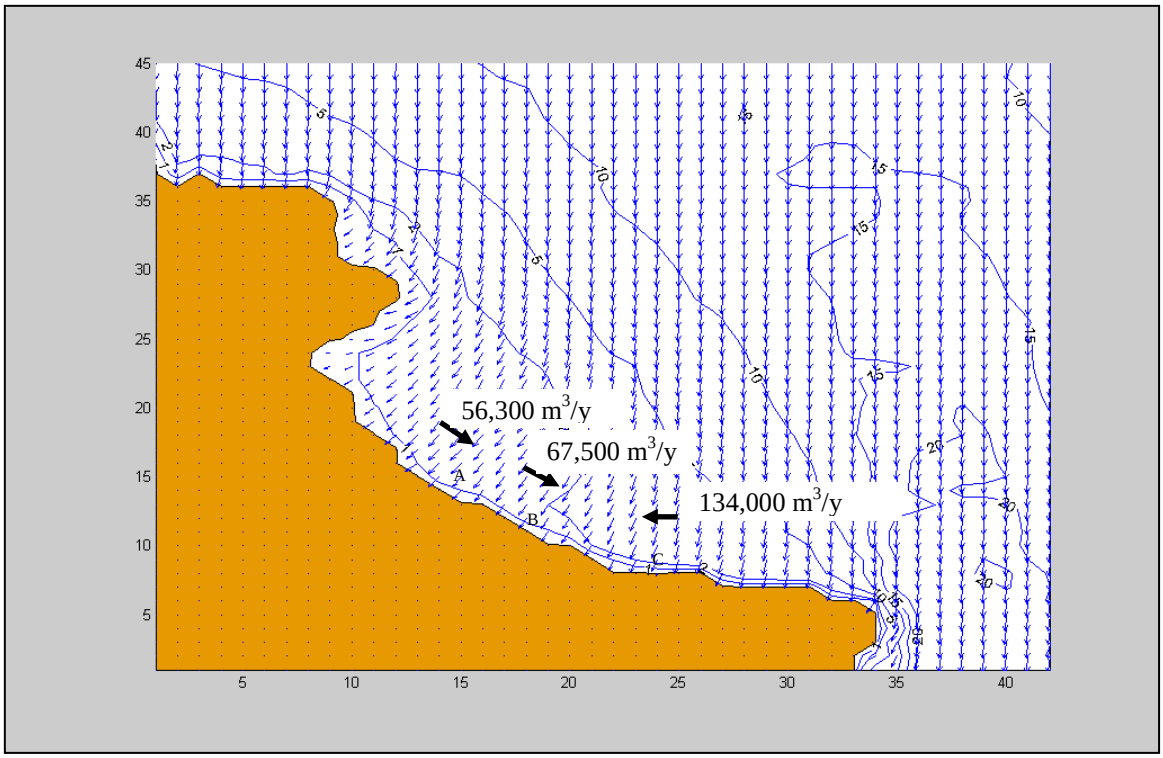

Figure 40 : Local sediment transport rate for case 5 before project with wave direction 0°, wave height 0.62 m, and wave period 2.79 s

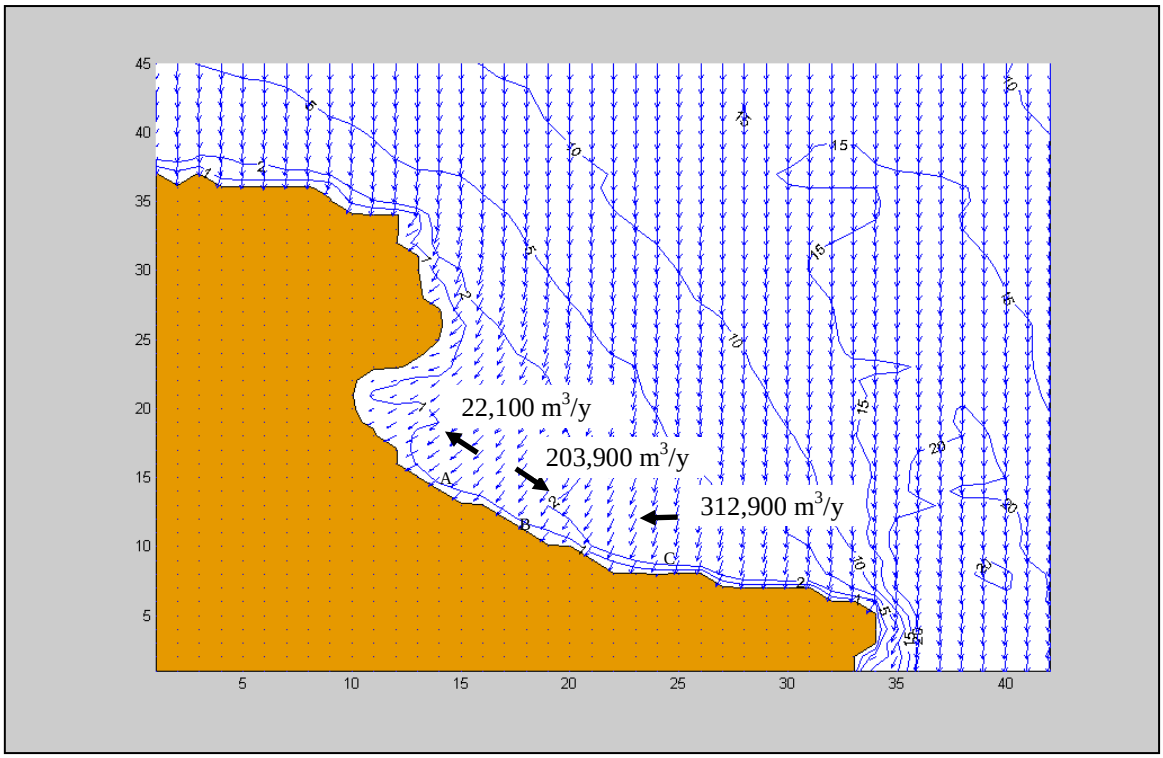

Figure 41 : Local sediment transport rate for case 6 after project with wave direction 0°, wave height 0.62 m, and wave period 2.79 s

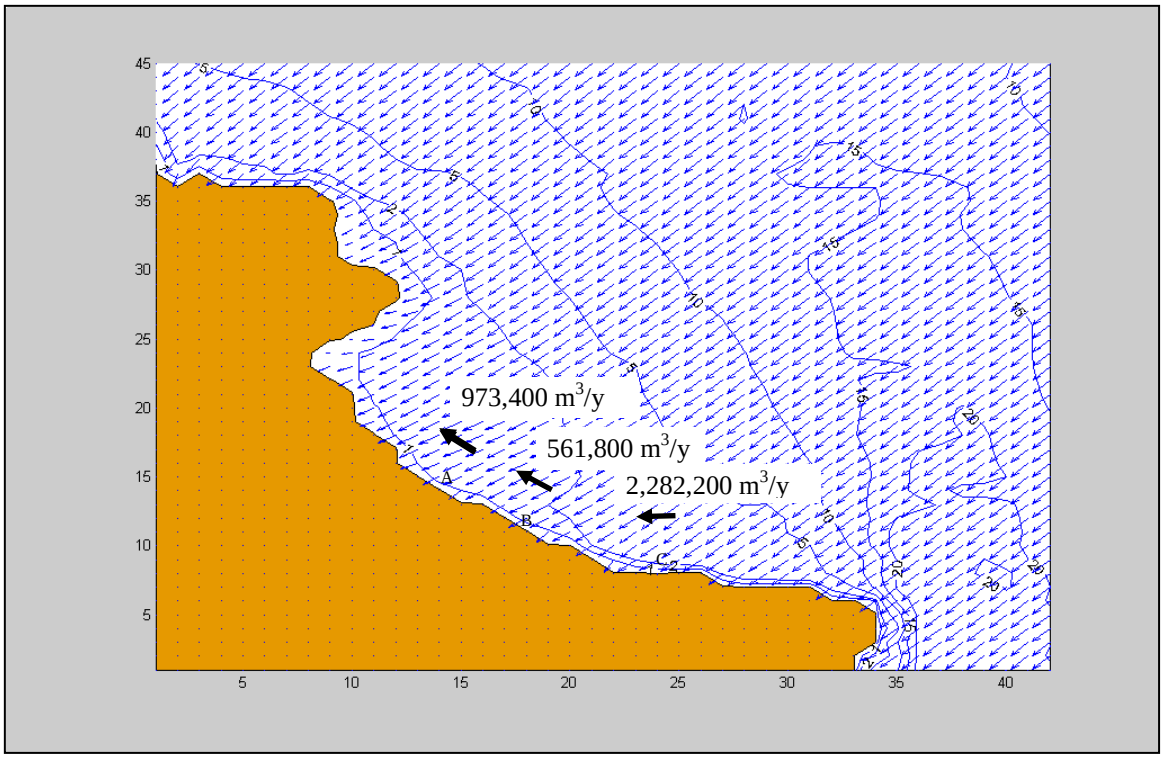

Figure 42 : Local sediment transport rate for case 7 before project with wave direction 40°, wave height 0.76 m, and wave period 3.38 s

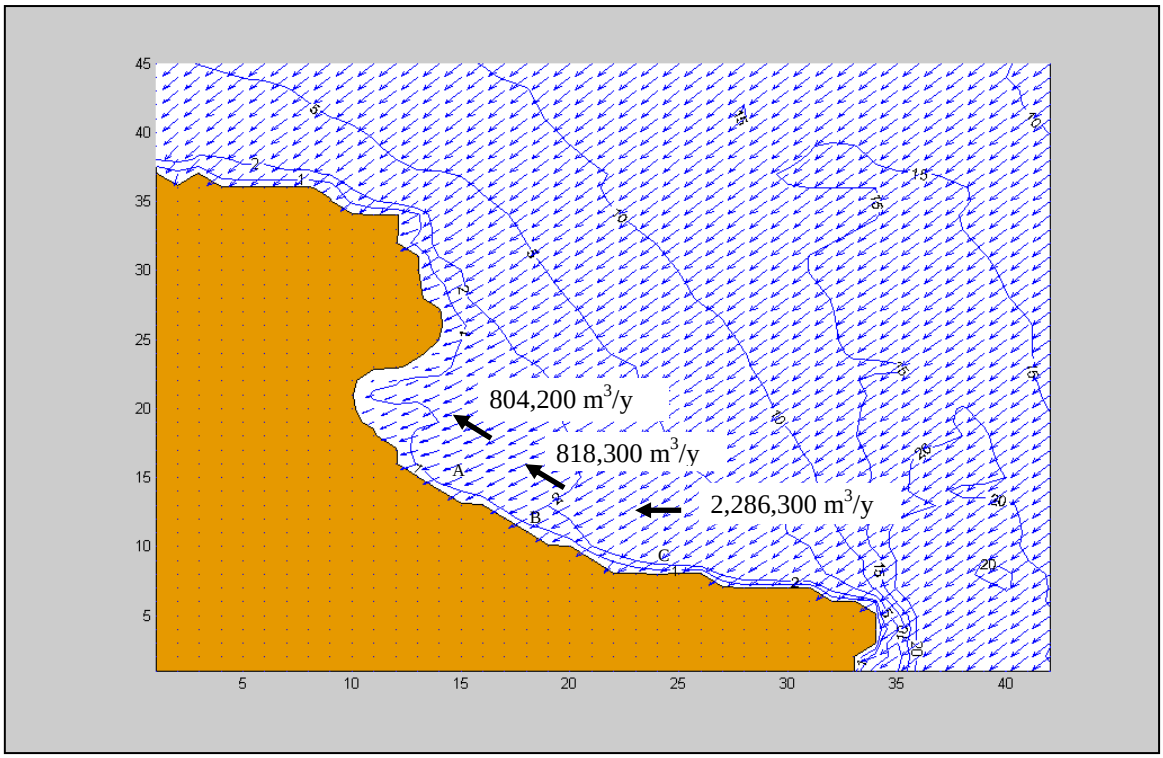

Figure 43 : Local sediment transport rate for case 8 after project with wave direction 40°, wave height 0.76 m, and wave period 3.38 s

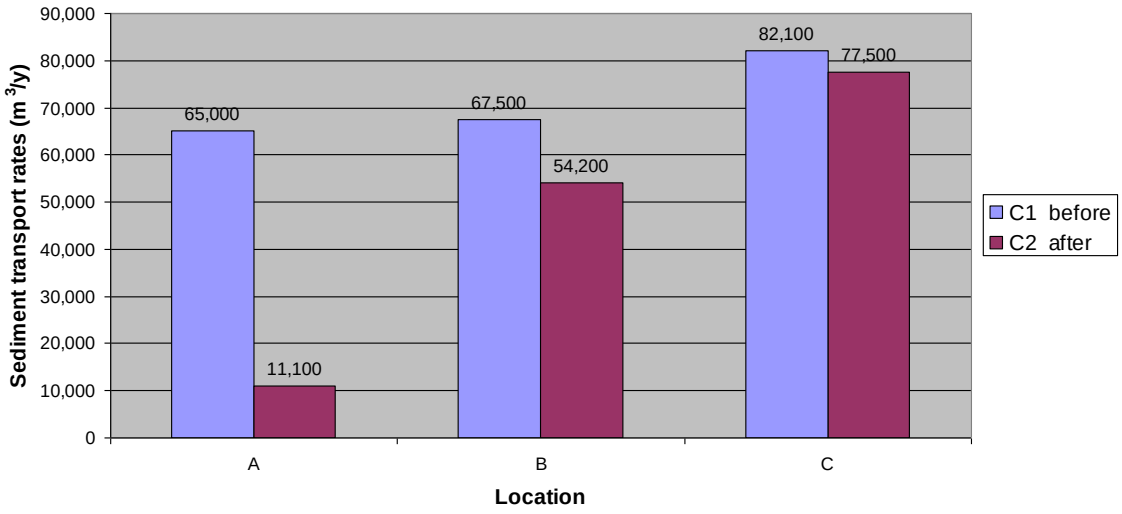

Figure 44 : Sediment transport rate before (case 1) and after (case 2) project at locations A, B, and C for incoming wave direction 280^{o}, H = 1.05m, and T =3.3s

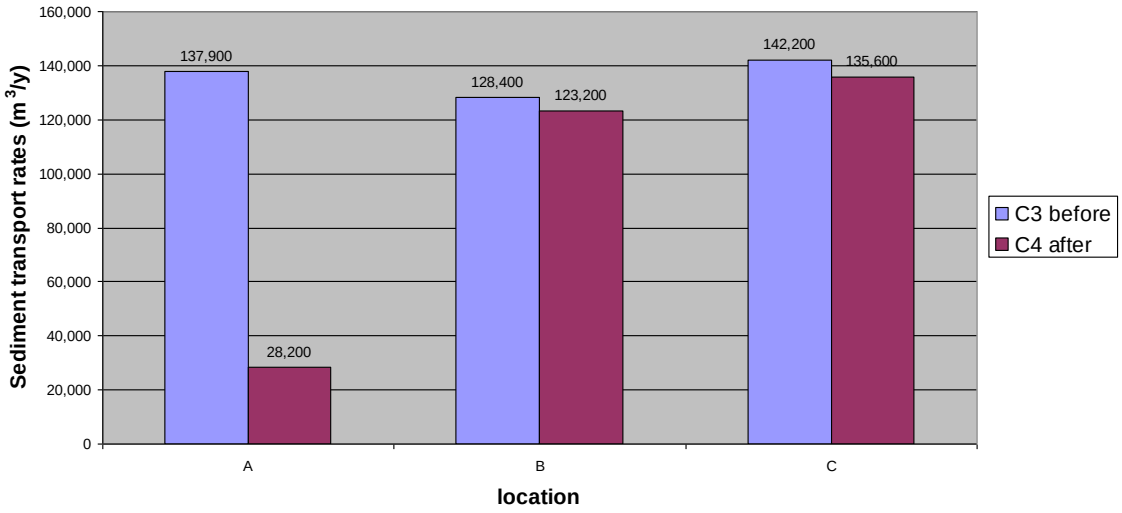

Figure 45 : Sediment transport rate before and after project at locations A, B, and C for incoming wave direction 320^{o}, H =0.73m, and T =3.1s

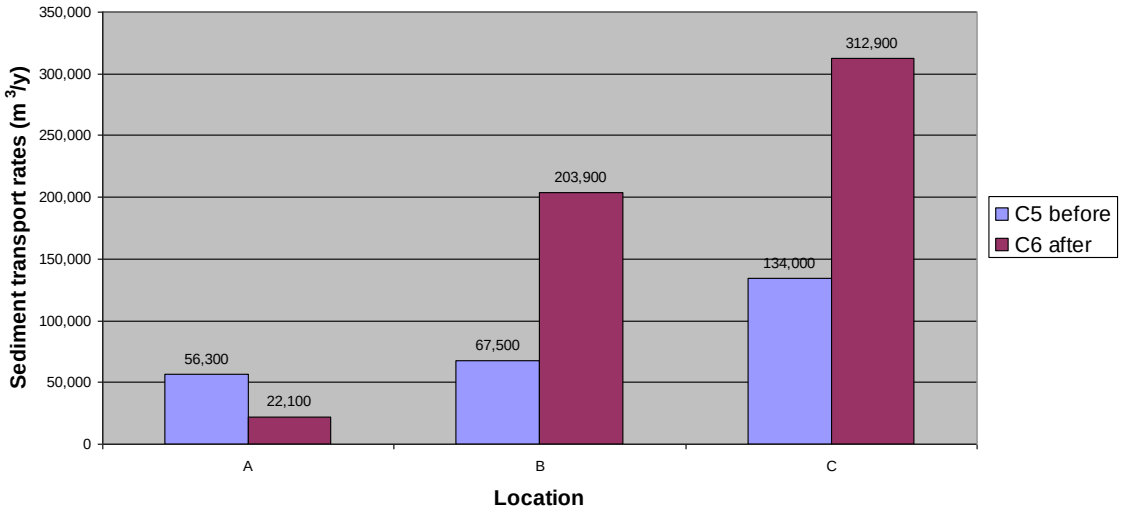

Figure 46 : Sediment transport rate before and after project at location, A, B, and C for incoming wave direction 0^{o}, H =0.62m, and T =2.79s

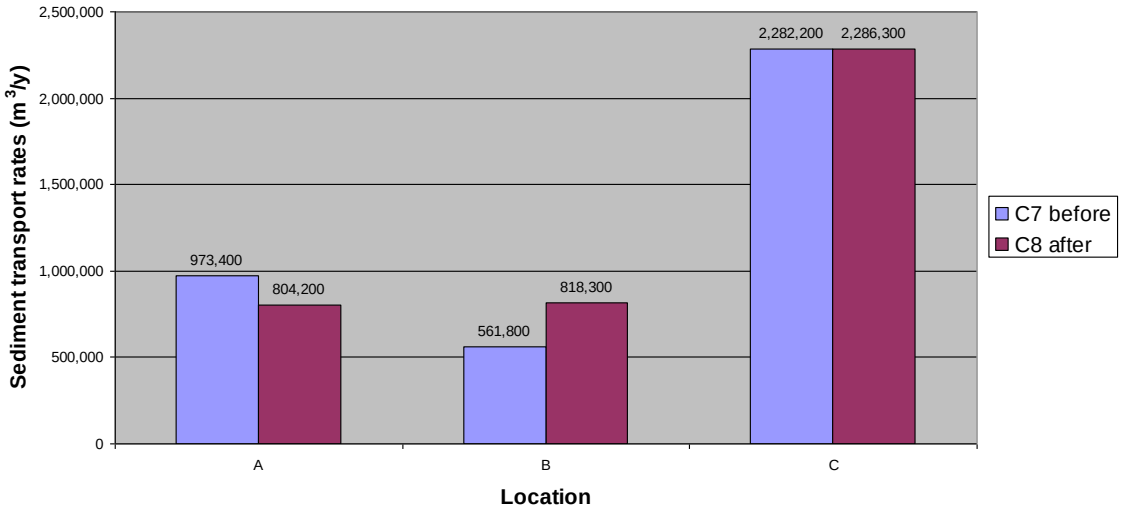

Figure 47 : Sediment transport rate before and after project at locations A, B, and C for incoming wave direction 40^{o}, H =0.76m, and T =3.38s

In general, from Figures 36 to 43 it can be seen that the local sediment transport directions did not differ so much for the situation after project compared to before the project. Only in the third scenario (Figure 40 and Figure 41) at location A, with incoming waves from the north, did the local sediment transport direction changed to the left after the project (direction of transport refers to a person standing on shore looking towards the sea, as before).

For incoming waves from the west, local sediment transport directions were towards the right side, whereas for incoming waves from the east, sediment transport directions were towards the left side both before and after project conditions. It seems that the local sediment transport direction for incoming waves from west and east were not significantly affected by the land reclamation project. Only for incoming waves from north, the local sediment transport at location A, which is the nearest to the project area, changed direction from right to left. This change occurred because the transformation of waves at location A, influenced by the land reclamation, changed the sediment transport direction for incoming waves from north condition.

Even though the wave transformation processes due to the land reclamation project did not cause any significant change in the local sediment transport direction, it influenced the local sediment transport rate. Figures 44 to Figure 47 show the differences in the local sediment transport rates before and after the project at locations A, B, and C for all four scenarios. These local sediment transport rates were calculated based on the hourly highest incident wave heights for each scenario and it were converted to meter cube per year. This rate is only representative for a storm and is not to be regarded as an annual value.

Figure 44 shows local sediment transport rates for the first scenario with the incoming wave direction 280^{o}. The local sediment transport rates decreased after the project. The most significantly affected location was at A, where the rate decreased 83% from $65{,}000m^3$/year to $11{,}000m^3$/year. Locations B and C also experienced 20% and 6% decline of local sediment transport rates corresponding to before project and after the project.

Comparison of local sediment transport rates at the three locations, C had the highest local sediment transport rate compared to locations A and B for both cases. For case 1, before the project, the sediment transport rate at C was $82{,}100m^3$/year, while it was $67{,}500m^3$/year at location B and $65{,}000m^3$/year at location A. After the project (case 2), the sediment transport rate at C was $77{,}500m^3$/year, $54{,}200m^3$/year at location B, and only $11{,}100m^3$/year at location A.

Local sediment transport rates for the second scenario are shown in Figure 45. With incoming waves at 320^{o} direction, local sediment transport rates after project decreased similarly to the first scenario. However, sediment transport rates for the second scenario were higher than the first scenario at all three locations before and after the project. Local sediment transport rate at location A after project decreased 79% from $137{,}900m^3$/year before project to $28{,}200m^3$/year after project and this was the most significantly affected location due to the implementation of the project. Locations B and C experienced less decrease in local sediment transport rates after the project with only 4% and 5% reduction, respectively.

In the case before project in the second scenario, there was not much difference in the sediment transport rate at locations A, B, and C. Location C had the highest local sediment transport rate followed by location A and B. For case 4 after project, location C

still had the highest local sediment transport rate followed by location B, whereas the rate at location A dropped drastically.

The third scenario in Figure 46 showed a different pattern of the local sediment transport simulation results. For the first and second scenario, the local sediment transport rate decreased after the implementation of the project. However, in the third scenario, with incoming waves from the north, sediment transport rate at locations C and B significantly increased after the project. Only location A experienced reduction in the sediment transport rate after the project from 56,300m^3/year to 22,100m3/year, and the sediment transport direction changed towards left side. Location C had the highest local sediment transport rate before and after the project. However, there was a large increase in the sediment transport rate at location B with a 67% increase from 67,500m^3/year before project to 203,900 m^3/year after project. Local sediment transport rate at location C increased 57 % from 134,000m^3/year before the project to 312,900m^3/year after the project.

In Figure 47, for the fourth scenario, with incoming waves from 40^o, it can be seen that there were slightly changes in the sediment transport rate after the project at locations A and B. Even though there was not much difference in the local sediment transport rate at location C before and after the project, the rate was large with more than 2,000,000 m^3/year before and after the project. The fourth scenario involved a very large amount of local sediment transport rate compared to the other scenarios. At location A, the local sediment rate decreased 17% with 973,400m^3/year before project to 804,200m^3/year after project. The opposite situation occurred at location B, where the local sediment transport rate after project increased 31% to 818,300m^3/year from 561,800m^3/year before project.

This analysis indicates that the local sediment transport rates are strongly influenced by the incoming wave direction and that the land reclamation project may impact the local sediment transport pattern. Sediment transport rate and direction play a role in the coastal evolution, which it will be discuss in next chapter.

6.3 Coastal evolution

As mentioned in previous section, the nearshore waves influence the sediment transport pattern and furthermore play a role in the coastal evolution. By knowing the nearshore sediment transport rate and its variation alongshore, the shoreline response can be predicted based on the transport gradients indicating either accumulation or erosion.

There were different patterns in the nearshore waves and sediment transport for different scenarios. Coastal evolution after the implementation of the project will be discussed accordingly for each scenario.

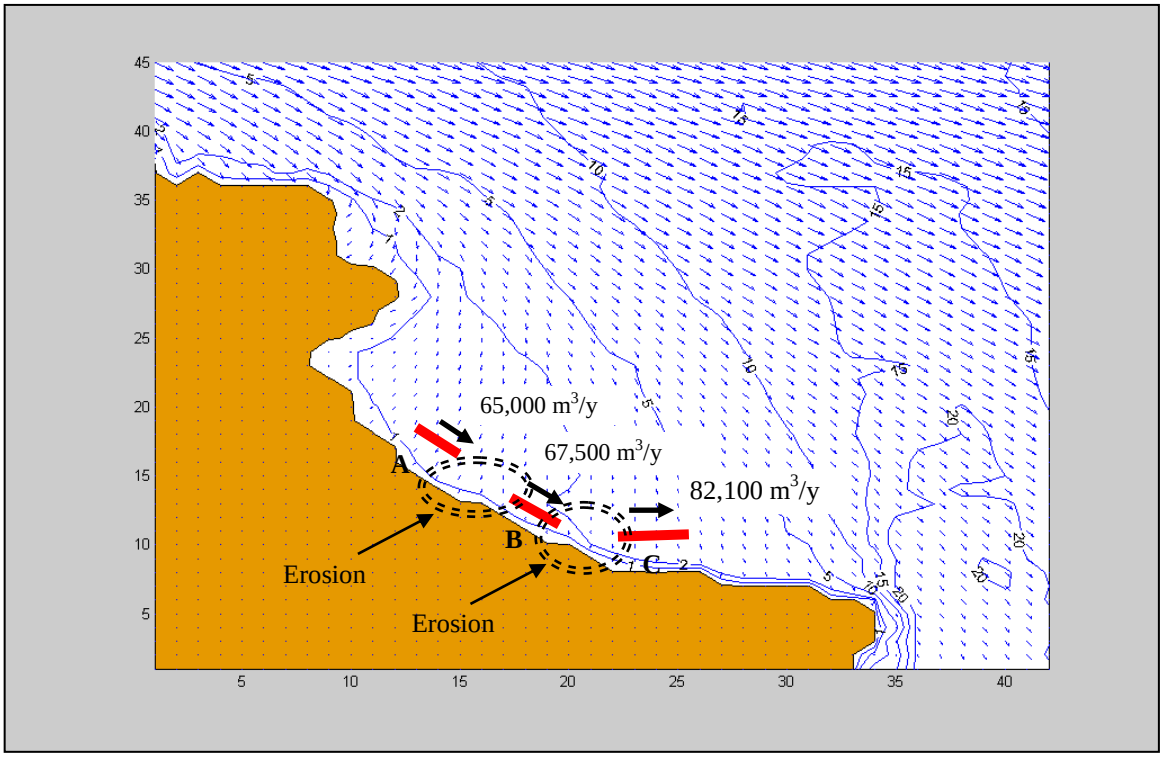

Figure 48 : Coastal evolution for the first scenario before land reclamation (Case 1)

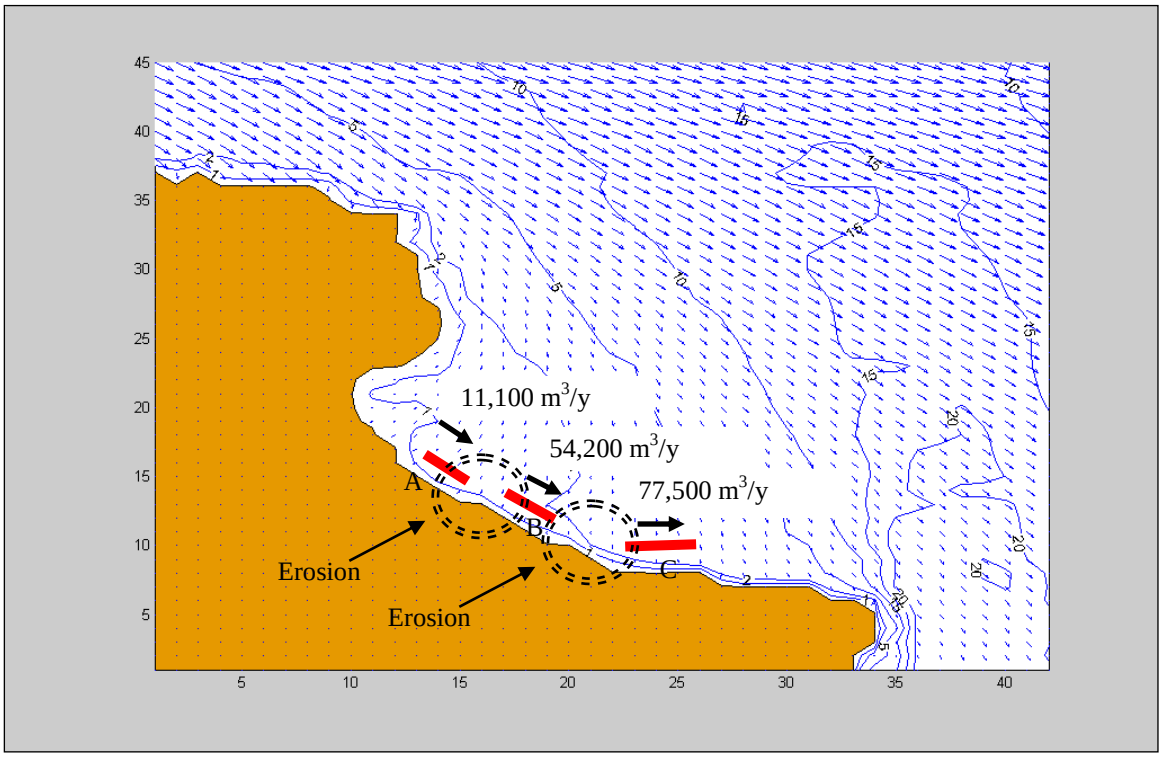

Figure 49 : Coastal evolution for the first scenario after land reclamation (Case 2)

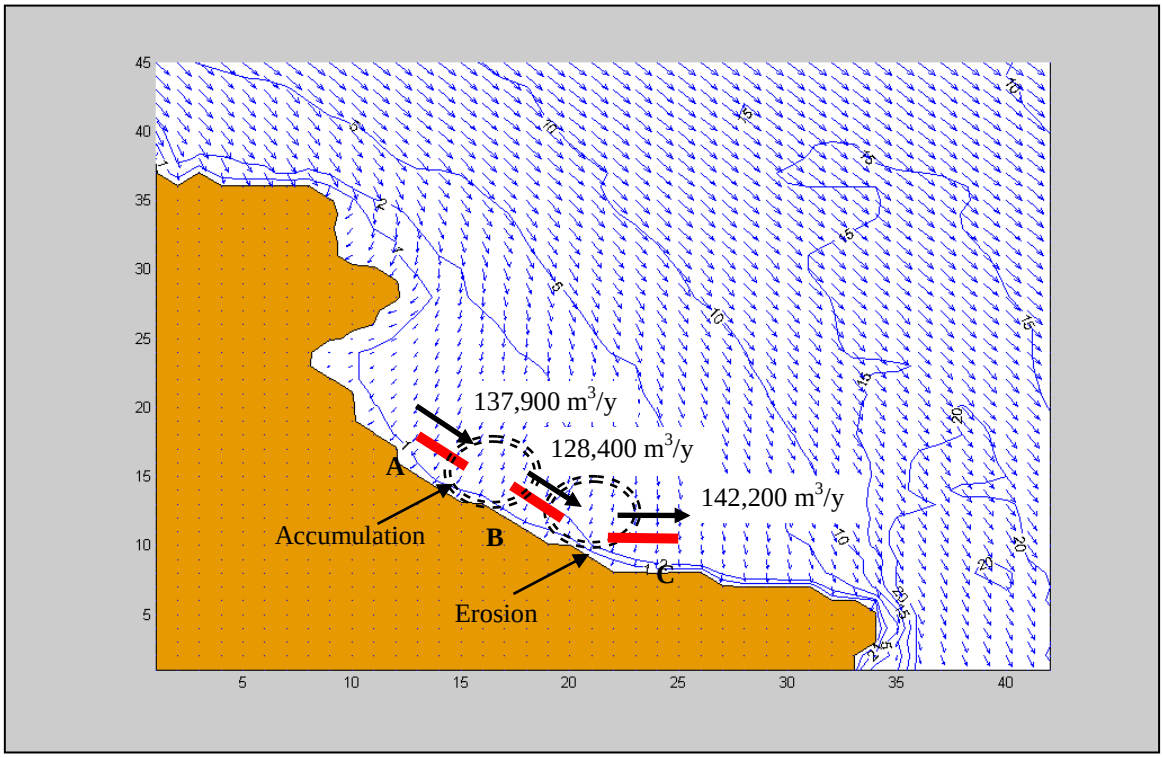

Figure 50 : Coastal evolution for the second scenario before land reclamation (Case 3)

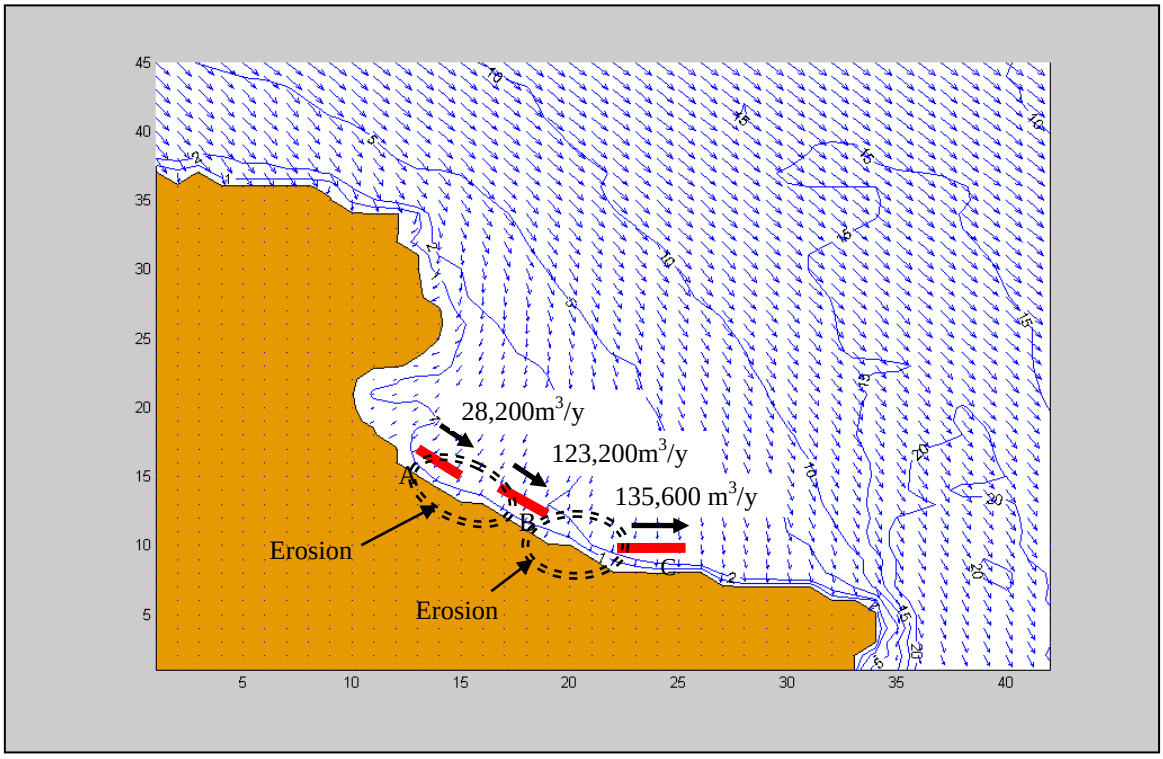

Figure 51 : Coastal evolution for the second scenario after land reclamation (Case 4)

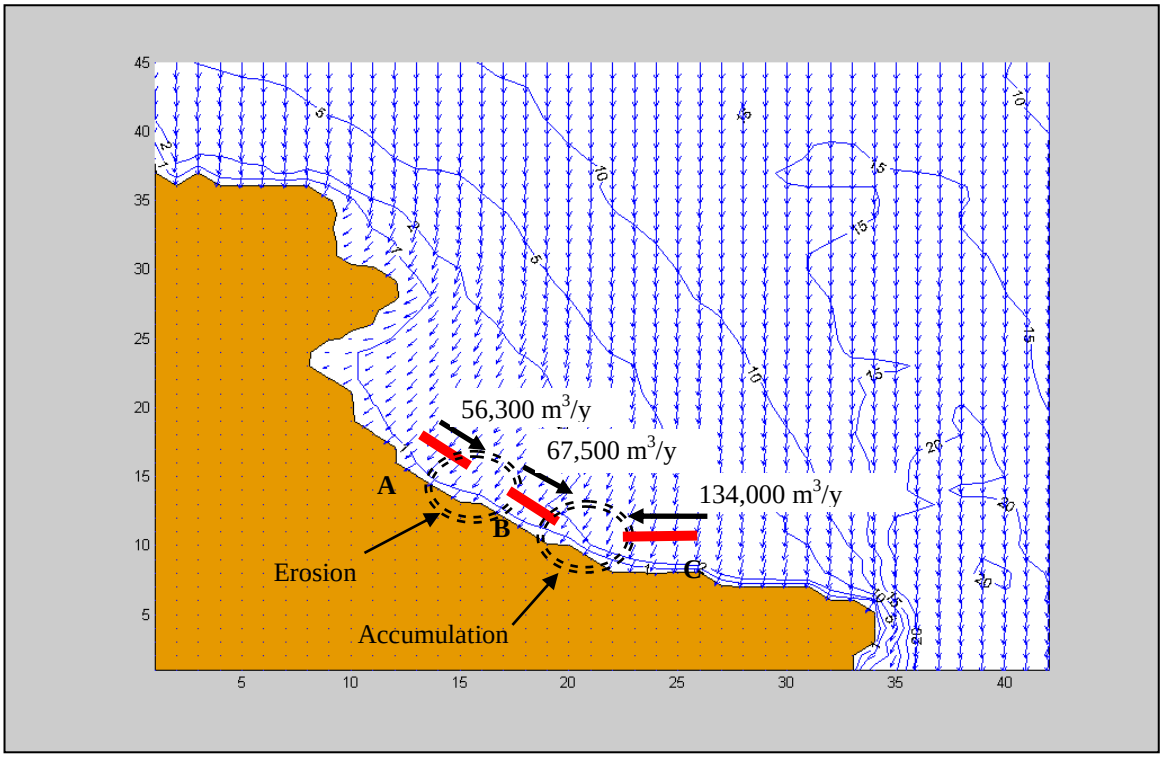

Figure 52 : Coastal evolution for third scenario before land reclamation (Case 5)

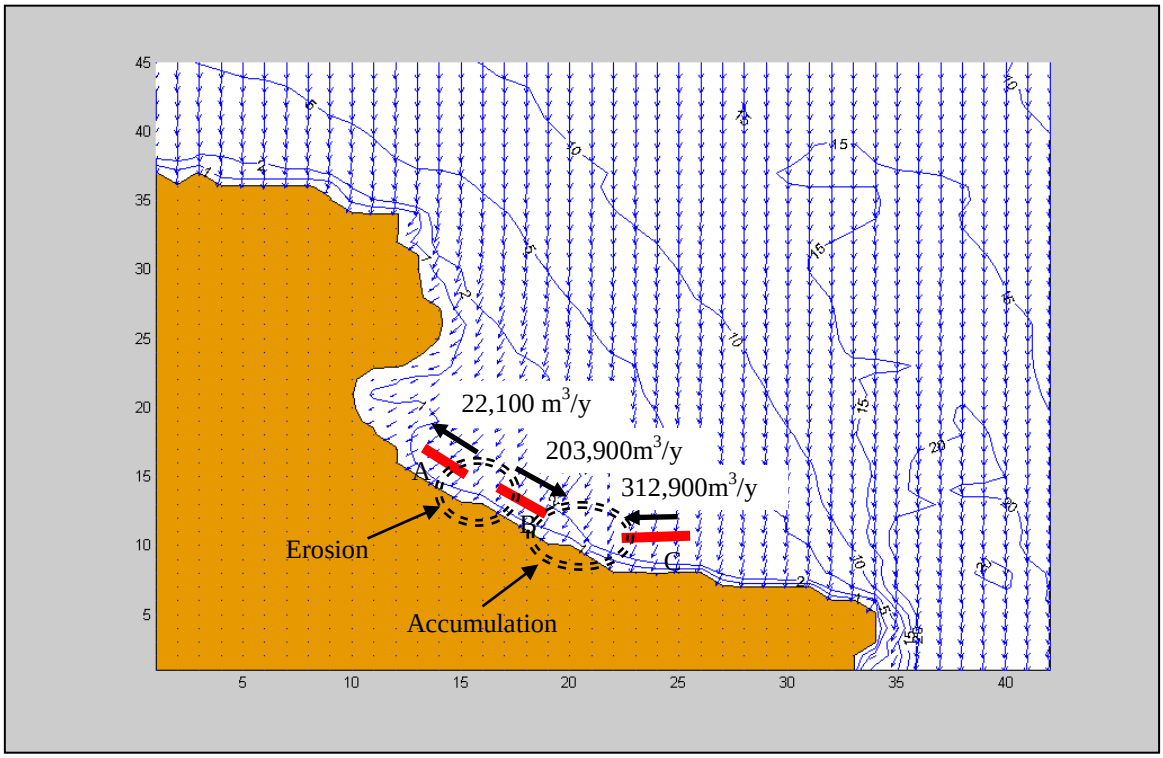

Figure 53 : Coastal evolution for third scenario after land reclamation (Case 6)

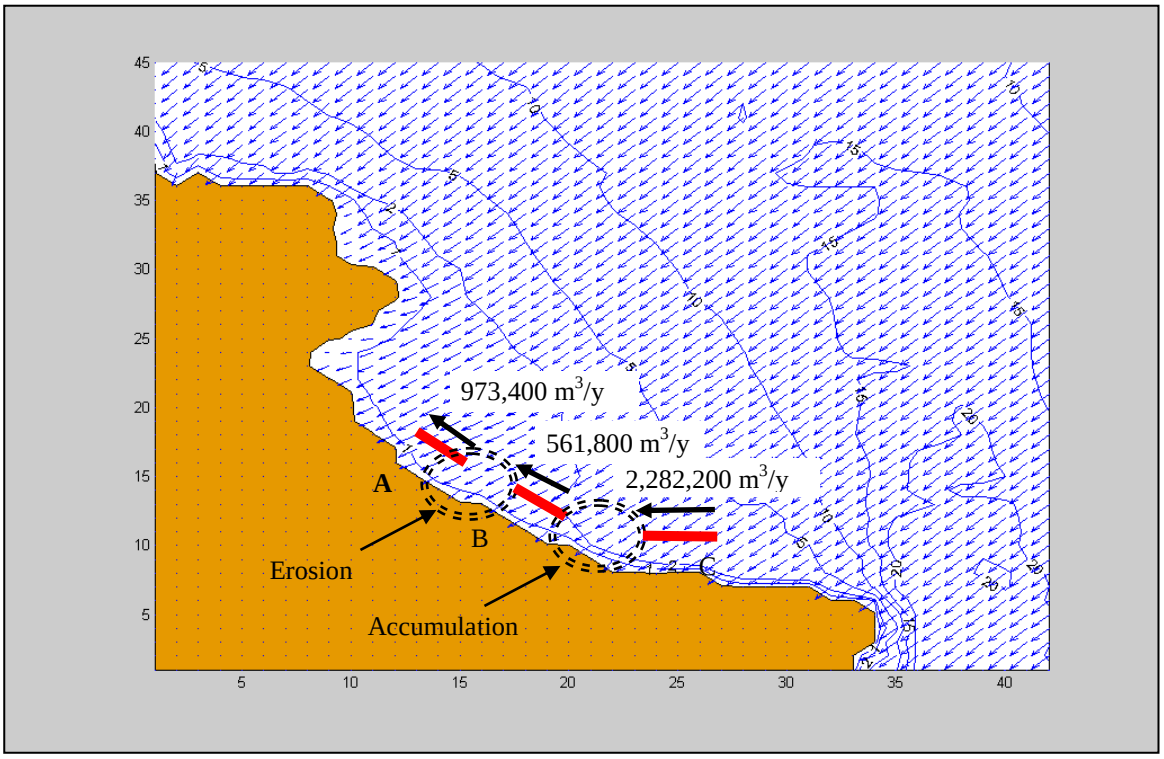

Figure 54 : Coastal evolution for fourth scenario before land reclamation (Case 7)

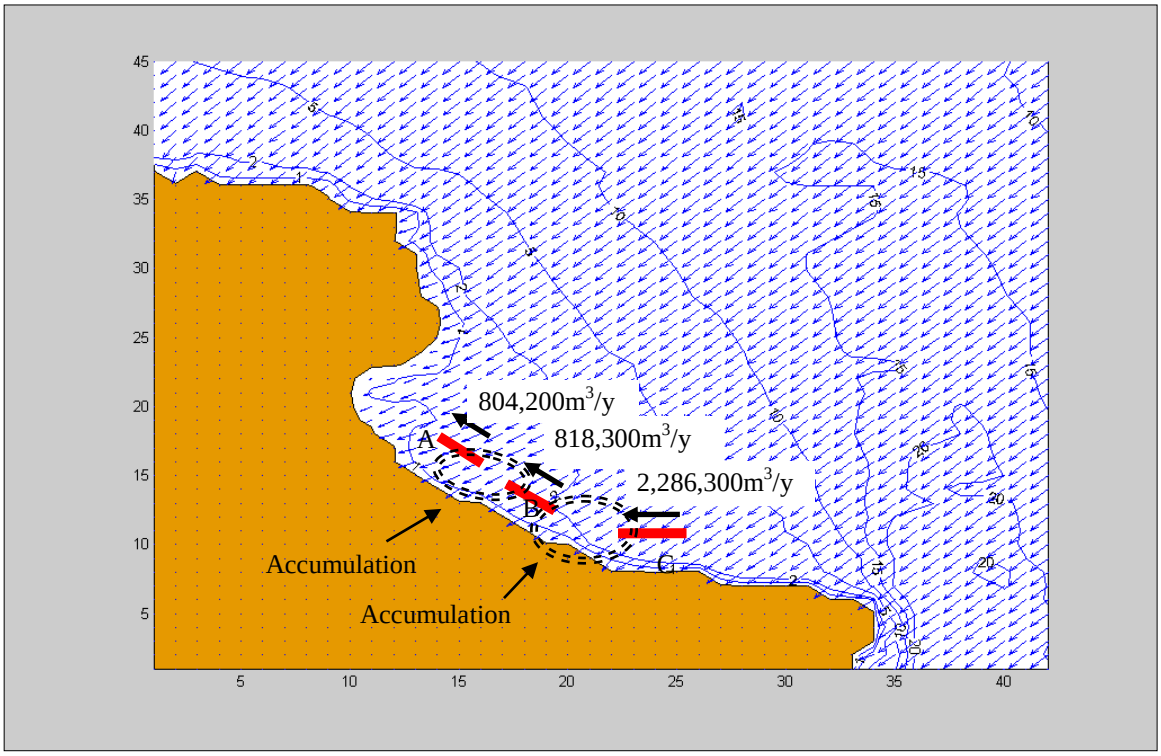

Figure 55 : Coastal evolution for fourth scenario after land reclamation (Case 8)

Figure 49 show the assessed coastal evolution for the first scenario after the land reclamation project. For the first scenario, the incoming wave direction was 280^{o} with significant wave height 1.06m and wave period was 3.3s. In general, sediment transport move to the right along shoreline. Since sediment transport rate at location C was higher than at location B, erosion will occur between locations B and C. The same situation will prevail between locations A and B, as sediment transport rate at location A was less than at location B. However, the erosion rate in the area between A and B would be higher than in the area between B and C. The rate of shoreline retreat is difficult to estimate, since the studied scenarios are representative of certain extreme events and their duration and probability is difficult to assess. So, the present analysis is more qualitative regarding the expected shoreline response. Compared to the situation before the project, the gradient between location A and B increases (see figure 48), implying that the amount of erosion increases in the area between A and B because of the fill.

In the second scenario, coastal evolution for incoming waves from 320^{o} is shown in Figure 51 after project. The pattern of coastal evolution in this scenario is the same as for the first scenario, where erosion is expected to occur between locations B and C, and also between locations B and A. The incoming waves from the west direction might be the reason for the similar pattern of coastal evolution for the first and second scenarios. Compared to the situation before the project in figure 50, a similar increase in the erosion between locations A and B is expected as for the first scenario.

There was a difference in the coastal evolution pattern for the third scenario compared to previous scenarios, as shown in figure 53. Longshore sediment transport direction at location A was to the left, whereas sediment at location B moved to right. This condition will induce erosion in the area between locations A and B. The opposite situation prevails between locations B and C. Accumulation is expected in this area because of the convergence of sediment from both locations B and C. In figure 52, the situation before the project also indicates erosion between A and B and accumulation between B and C. However, the erosion between A and B before the project is due to an increased alongshore transport gradient, whereas after the fill a point of sediment divergence occurs in this area.

For the fourth scenario with incoming waves from 40^{o}, accumulation will occur in study area as can be seen in figure 55. The sediment direction at locations A, B, and C is to the left with the sediment rate at location C being the highest, followed by the sediment rate at location B, and then at location A. When the incoming sediment transport rate to an area is larger than the outgoing rate, accumulation will take place. Before the project (figure 54) the area between locations A and B will experience erosion, which is different from the predicted conditions after the project.

Incoming waves from the offshore determines the nearshore sediment patterns, giving rise to coastal morphological changes through the gradients induced in the transport rate. In this study, incoming waves from the west caused local sediment directions that have a

tendency to move sediment to the right along the shore. Meanwhile, local sediment moves to the left for incoming waves from the east. South of the land reclamation, erosion is expected for incoming waves from the west, whereas accumulation occurs for waves from the east, the latter probably being more significant.

7. Conclusions

The aims of this study were achieved in terms of understanding and quantifying wave transformation and sediment transport processes along the shore and assessing the effects of the land reclamation on the coastal areas. However, environment and ecosystems aspects are not included in this study. To begin with, general coastal processes in Penang were investigated and the project background described to get an overview of the study area. Then, a numerical model, EBED, was employed to simulate the nearshore wave transformation in the specified study area for four different scenarios of incident wave heights and wave directions before and after the project.

From the results of calculations in this study, there were noticeable impacts on the coastal areas after the Tanjung Tokong Land Reclamation project concerning the wave transformation patterns, the longshore sediment transport rates, and the associated shoreline responses.

The results show that the wave direction changed after the project. Land reclamation caused changes at shoreline by enlarge the land area towards the sea influencing the wave transformation behaviour. The most affected area was at study location A, which is at the nearest location to the project area. Wave transformation in the nearshore occurs because of diffraction, refraction, and shoaling processes that the waves undergo when they travel to the shore. After construction of the project, the transformation of the waves coming from the west was more significantly affected compared to the waves coming from the north and east. Therefore, changes in shoreline alignment and sea bed contours due to the project affected the wave transformation.

Local sediment transport directions in the nearshore areas did not differ a lot before and after the project. The transport directions for incoming waves from the west and east did not change after the project. However, the local sediment transport rates significantly changed after project depending on the incoming wave direction.

Based on local sediment transport rates and directions in the study area, the coastal evolution was predicted based on the transport gradients indicating either erosion or accumulation after the project in the studied areas. Incoming waves from the west caused local sediment directions that displayed a tendency to move sediment to the right along the shore. Meanwhile, local sediment for incoming waves from the east would move sediment to left side along the shoreline. Erosion was expected for incoming waves from the west and accumulation for incoming waves from the east. The sediment transport patterns before and after the project were similar. However, the gradients were larger in the areas immediately south of the fill after the project, indicating larger changes here.

As a conclusion, the study showed that Tanjung Tokong Land Reclamation Project will have an impact on the wave transformation, sediment transport, and coastal evolution in the studied areas, although further investigations are needed to better quantify this impact, especially for the coastal evolution.

References

Angelbratt A., Klüft J., 2007, Seasonal Closure of Chilaw Inlet in Sri Lanka - Physical Processes and Mathematical Modelling, Master Thesis, Lund University.

Bayram A., Larson M., Hanson H., 2007, A new formula for the total longshore sediment transport rate, *Ocean Engineering* [Online] 54 (2007) 700–710
Available at: http:// www.elsevier.com [accessed 9 October 2007]

CEM, 2002, Coastal Engineering Manual, Coastal and Hydraulics Laboratory, Engineer Research and Development Center, Vickburg, Mississippi.

Emanuelsson D., Mirchi A., 2007, Impact of coastal erosion and sedimentation along the Northern Coast of Sinai Peninsula, Master Thesis, Lund University.

Häglund M., Svensson P., 2002, Coastal Erosion at Hau Hau Beach in the Red River Delta, Vietnam, Master Thesis, Lund University.

Mase H., Oki K., Hedges T. S. & Li H. J., 2004, Extended energy-balance-equation wave model for multidirectional random wave transformation, *Ocean Engineering* [Online] 32 (2005) 961–985
Available at: http:// www.elsevier.com [accessed 16 October 2007]

Mase H., 2001, Multi-directional random wave transformation model based on energy balance equation, *Coastal Engineering Journal* [Online] Vol. 43, No. 4 (2001) 317-337.
Available at: http:// www.elsevier.com [accessed 16 October 2007]

Tanjung Pinang Development Sdn Bhd (TPD), 2003, Tanjung Pinang Development Land Reclamation Project – Phase 1, Coastal Engineering and Hydraulic Study, Dr. Nik & Associates Sdn Bhd, Kuala Lumpur.

SPM, 1984, Shore Protection Manual, Department of Army, Coastal Engineering Research Center, Vickburg, Mississippi.

Malaysian Meteorology Department (MMD), Climate of Malaysia
Available at http://www.met.gov.my/home_e.html [accessed 8 November 2007]

Appendix 1 : Annual wind rose at Butterworth from 1971-1990. Data is from Department of Irrigation and Drainage Malaysia

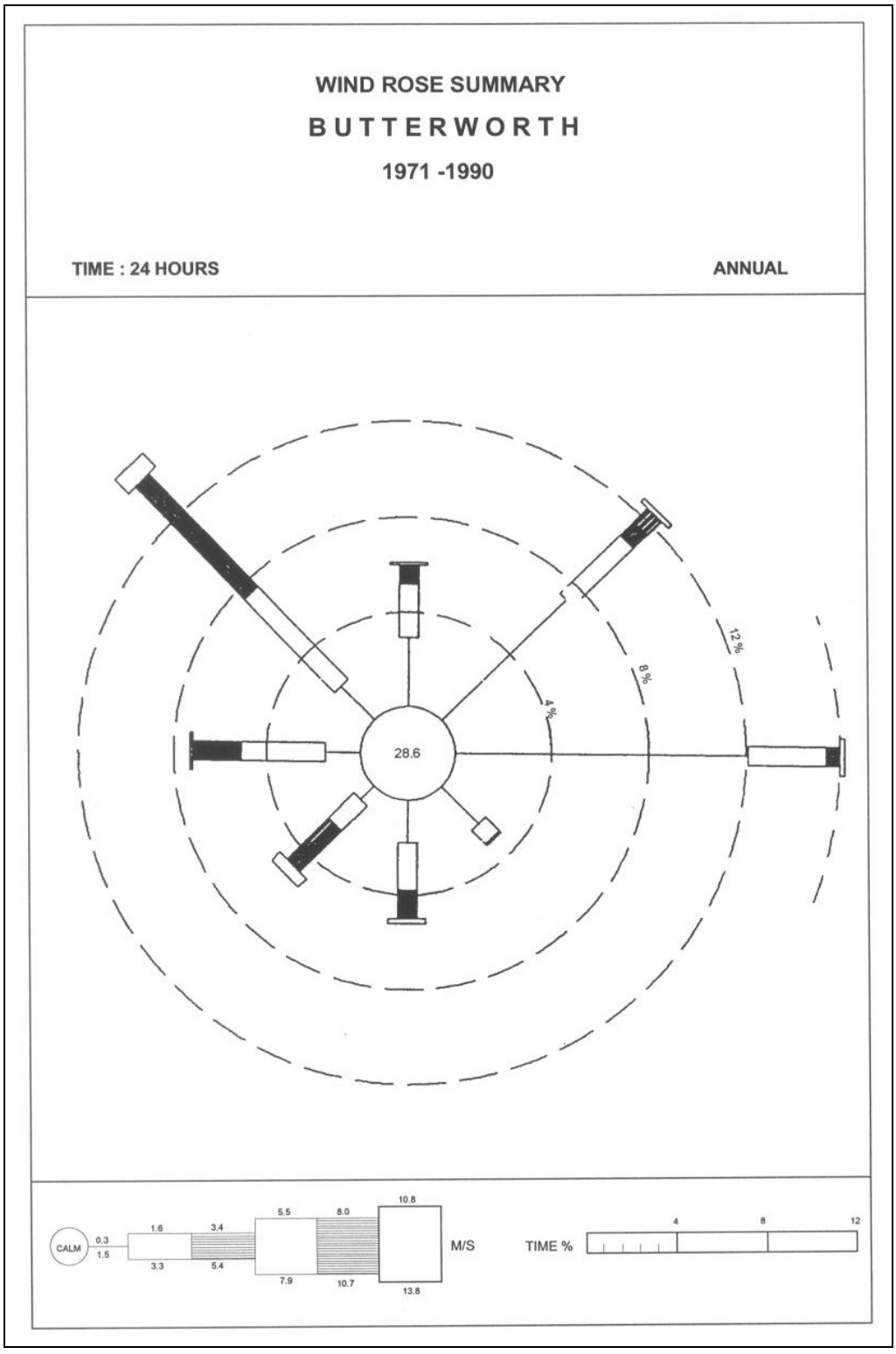

Appendix 2 : Seasonal wind roses at Butterworth for year 1985 to year 1990

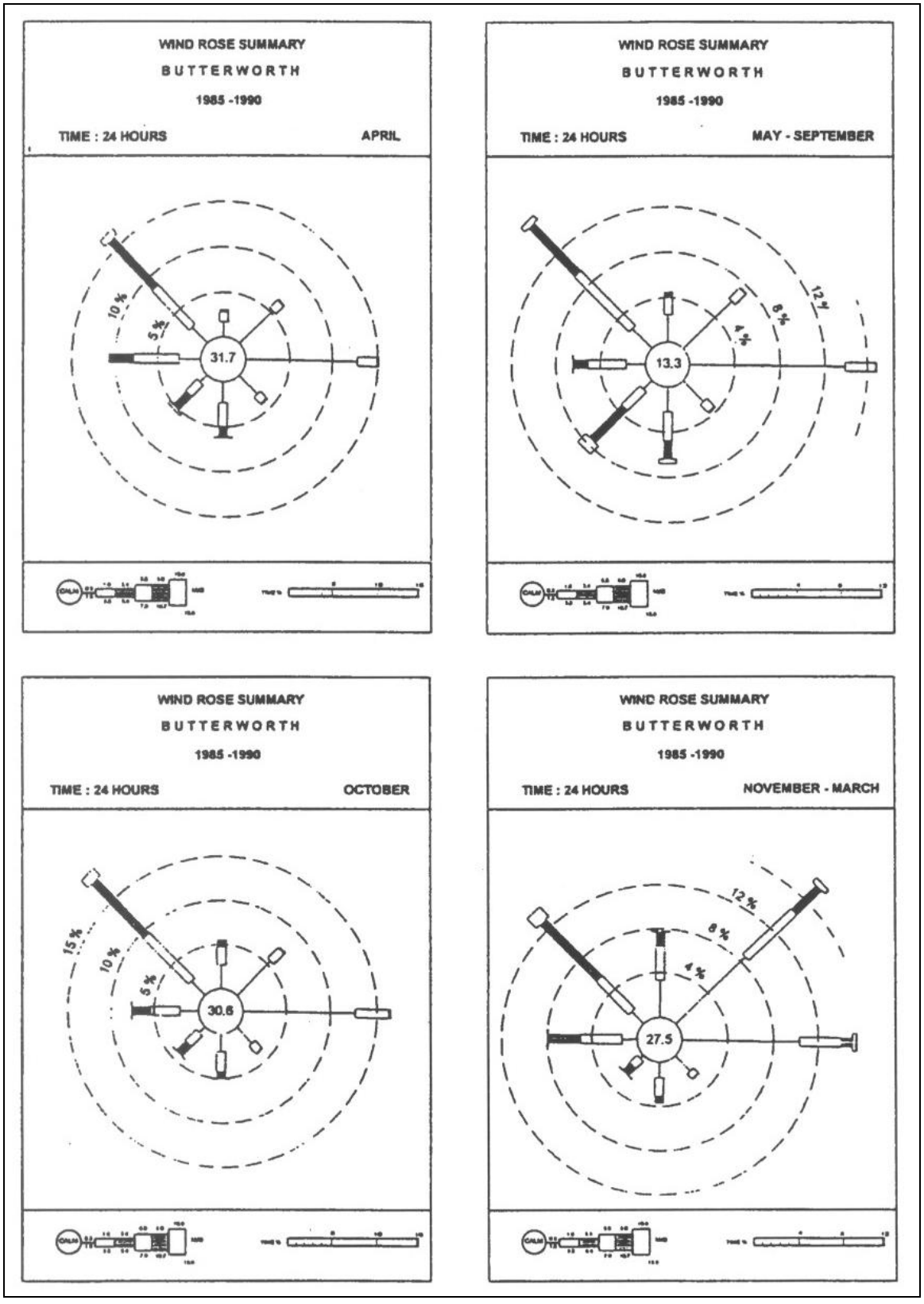

Appendix 3 : Wave statistics summaries at Penang from 01-01-1958 to 31-12-1984

BAHAGIAN KEJURUTERAAN PANTAI
JABATAN PENGAIRAN DAN SALIRAN MALAYSIA
WAVE STATISTICS SUMMARIES - WAVE & SWELL

MARSDEN SQUARE : 2640 2650 2660 2748 2749 2756 2757 2758 2759 2766 2767 2768 2769
STARTING DATE : 01-01-1958 ENDING DATE : 31-12-1984
NO. OBSERVATIONS : 13481 PERCENT CALM : 0.00%
CHOSEN MONTHS : JAN FEB MAC APR MAY JUN JUL AUG SEP OCT NOV DEC

Direction : 345 - 015 DEGREES

	1	2	3	4	5	6	Total
1	3.8	0.1	0.0	0.0	0.0	0.0	3.9
2	1.4	0.1	0.0	0.0	0.0	0.1	1.6
3	0.3	0.1	0.0	0.0	0.0	0.0	0.4
4	0.1	0.1	0.0	0.0	0.0	0.0	0.1
5	0.0	0.0	0.0	0.0	0.0	0.0	0.0
6	0.0	0.0	0.0	0.0	0.0	0.0	0.1
7	0.0	0.0	0.0	0.0	0.0	0.0	0.0
8	0.0	0.0	0.0	0.0	0.0	0.0	0.0
9	0.0	0.0	0.0	0.0	0.0	0.0	0.1
Total	5.5	0.4	0.0	0.1	0.0	0.1	6.2

Direction : 015 - 045 DEGREES

	1	2	3	4	5	6	Total
1	4.2	0.1	0.0	0.0	0.0	0.1	4.4
2	1.7	0.3	0.1	0.0	0.0	0.1	2.2
3	0.8	0.3	0.1	0.0	0.0	0.0	1.1
4	0.1	0.1	0.1	0.0	0.0	0.0	0.3
5	0.0	0.0	0.0	0.0	0.0	0.0	0.0
6	0.0	0.0	0.0	0.0	0.0	0.0	0.1
7	0.0	0.0	0.0	0.0	0.0	0.0	0.0
8	0.0	0.0	0.0	0.0	0.0	0.0	0.0
9	0.0	0.0	0.0	0.0	0.0	0.0	0.1
Total	6.8	0.8	0.2	0.1	0.0	0.2	8.1

LEGENDS :

PERIOD CODE (IN SECONDS)
1= 4-5, 2= 6-7, 3= 8-9, 4= 10-11, 5= 12-13, 6= >13

WAVE HEIGHT CODE (IN METERS)
1= < 0.75, 2= 0.75-1.25, 3= 1.25-1.75, 4= 1.75-2.25, 5= 2.25-2.75, 6= 2.75-3.25, 7= 3.25-3.75, 8= 3.75-4.25, 9= >4.25

Page : 1

BAHAGIAN KEJURUTERAAN PANTAI
JABATAN PENGAIRAN DAN SALIRAN MALAYSIA
WAVE STATISTICS SUMMARIES - WAVE & SWELL

MARSDEN SQUARE : 2640 2650 2660 2748 2749 2756 2757 2758 2759 2766
2767 2768 2769
STARTING DATE : 01-01-1958 ENDING DATE : 31-12-1984
NO. OBSERVATIONS : 13481 PERCENT CALM : 0.00%
CHOSEN MONTHS : JAN FEB MAC APR MAY JUN JUL AUG SEP OCT NOV DEC

Direction : 045 - 075 DEGREES

	1	2	3	4	5	6	Total
1	4.7	0.2	0.0	0.0	0.0	0.1	5.0
2	3.1	0.5	0.1	0.0	0.0	0.1	3.8
3	1.2	0.4	0.1	0.0	0.0	0.1	1.9
4	0.5	0.2	0.0	0.0	0.0	0.0	0.8
5	0.1	0.1	0.0	0.0	0.0	0.0	0.2
6	0.0	0.0	0.0	0.0	0.0	0.0	0.0
7	0.0	0.0	0.0	0.0	0.0	0.0	0.0
8	0.0	0.0	0.0	0.0	0.0	0.0	0.0
9	0.0	0.0	0.0	0.0	0.0	0.0	0.1
Total	9.6	1.5	0.3	0.2	0.1	0.3	11.9

Direction : 075 - 105 DEGREES

	1	2	3	4	5	6	Total
1	4.5	0.1	0.0	0.0	0.0	0.0	4.7
2	2.4	0.3	0.1	0.0	0.0	0.1	3.0
3	0.9	0.3	0.0	0.0	0.0	0.0	1.3
4	0.2	0.2	0.1	0.0	0.0	0.0	0.4
5	0.1	0.1	0.0	0.0	0.0	0.0	0.2
6	0.0	0.0	0.0	0.0	0.0	0.0	0.0
7	0.0	0.0	0.0	0.0	0.0	0.0	0.0
8	0.0	0.0	0.0	0.0	0.0	0.0	0.0
9	0.1	0.0	0.0	0.0	0.0	0.0	0.1
Total	8.2	0.9	0.2	0.1	0.0	0.2	9.7

LEGENDS :

PERIOD CODE (IN SECONDS)
1= 4-5, 2= 6-7, 3= 8-9, 4= 10-11, 5= 12-13, 6= >13

WAVE HEIGHT CODE (IN METERS)
1= < 0.75, 2= 0.75-1.25, 3= 1.25-1.75, 4= 1.75-2.25, 5= 2.25-2.75,
6= 2.75-3.25, 7= 3.25-3.75, 8= 3.75-4.25, 9= >4.25

BAHAGIAN KEJURUTERAAN PANTAI
JABATAN PENGAIRAN DAN SALIRAN MALAYSIA
WAVE STATISTICS SUMMARIES - WAVE & SWELL

MARSDEN SQUARE : 2640 2650 2660 2748 2749 2756 2757 2758 2759 2766
2767 2768 2769
STARTING DATE : 01-01-1958 ENDING DATE : 31-12-1984
NO. OBSERVATIONS : 13481 PERCENT CALM : 0.00%
CHOSEN MONTHS : JAN FEB MAC APR MAY JUN JUL AUG SEP OCT NOV DEC

Direction : 105 - 135 DEGREES

	1	2	3	4	5	6	Total
1	3.3	0.1	0.0	0.0	0.0	0.0	3.5
2	1.3	0.1	0.0	0.0	0.0	0.0	1.5
3	0.3	0.1	0.0	0.0	0.0	0.0	0.4
4	0.1	0.0	0.0	0.0	0.0	0.0	0.1
5	0.0	0.0	0.0	0.0	0.0	0.0	0.0
6	0.0	0.0	0.0	0.0	0.0	0.0	0.0
7	0.0	0.0	0.0	0.0	0.0	0.0	0.0
8	0.0	0.0	0.0	0.0	0.0	0.0	0.0
9	0.0	0.0	0.0	0.0	0.0	0.0	0.1
Total	5.0	0.3	0.1	0.1	0.0	0.1	5.6

Direction : 135 - 165 DEGREES

	1	2	3	4	5	6	Total
1	2.6	0.1	0.0	0.0	0.0	0.0	2.8
2	1.0	0.1	0.0	0.0	0.0	0.0	1.2
3	0.2	0.1	0.0	0.0	0.0	0.0	0.3
4	0.1	0.0	0.0	0.0	0.0	0.0	0.1
5	0.0	0.0	0.0	0.0	0.0	0.0	0.0
6	0.0	0.0	0.0	0.0	0.0	0.0	0.0
7	0.0	0.0	0.0	0.0	0.0	0.0	0.0
8	0.0	0.0	0.0	0.0	0.0	0.0	0.0
9	0.0	0.0	0.0	0.0	0.0	0.0	0.1
Total	3.9	0.3	0.0	0.1	0.1	0.1	4.5

LEGENDS :

PERIOD CODE (IN SECONDS)
1= 4-5, 2= 6-7, 3= 8-9, 4= 10-11, 5= 12-13, 6= >13

WAVE HEIGHT CODE (IN METERS)
1= < 0.75, 2= 0.75-1.25, 3= 1.25-1.75, 4= 1.75-2.25, 5= 2.25-2.75,
6= 2.75-3.25, 7= 3.25-3.75, 8= 3.75-4.25, 9= >4.25

BAHAGIAN KEJURUTERAAN PANTAI
JABATAN PENGAIRAN DAN SALIRAN MALAYSIA
WAVE STATISTICS SUMMARIES - WAVE & SWELL

MARSDEN SQUARE : 2640 2650 2660 2748 2749 2756 2757 2758 2759 2766
2767 2768 2769
STARTING DATE : 01-01-1958 ENDING DATE : 31-12-1984
NO. OBSERVATIONS : 13481 PERCENT CALM : 0.00%
CHOSEN MONTHS : JAN FEB MAC APR MAY JUN JUL AUG SEP OCT NOV DEC

Direction : 165 - 195 DEGREES

	1	2	3	4	5	6	Total
1	2.0	0.0	0.0	0.0	0.0	0.0	2.1
2	0.6	0.1	0.1	0.0	0.0	0.0	0.8
3	0.1	0.0	0.0	0.0	0.0	0.0	0.2
4	0.0	0.0	0.0	0.0	0.0	0.0	0.1
5	0.0	0.0	0.0	0.0	0.0	0.0	0.1
6	0.0	0.0	0.0	0.0	0.0	0.0	0.0
7	0.0	0.0	0.0	0.0	0.0	0.0	0.0
8	0.0	0.0	0.0	0.0	0.0	0.0	0.0
9	0.0	0.0	0.0	0.0	0.0	0.0	0.0
Total	2.7	0.3	0.2	0.1	0.0	0.1	3.3

Direction : 195 - 225 DEGREES

	1	2	3	4	5	6	Total
1	2.2	0.0	0.0	0.0	0.0	0.0	2.3
2	0.7	0.1	0.0	0.0	0.0	0.0	0.9
3	0.1	0.1	0.0	0.0	0.0	0.0	0.3
4	0.1	0.1	0.0	0.0	0.0	0.0	0.2
5	0.0	0.0	0.0	0.0	0.0	0.0	0.0
6	0.0	0.0	0.0	0.0	0.0	0.0	0.0
7	0.0	0.0	0.0	0.0	0.0	0.0	0.0
8	0.0	0.0	0.0	0.0	0.0	0.0	0.0
9	0.0	0.0	0.0	0.0	0.0	0.0	0.0
Total	3.1	0.4	0.2	0.1	0.0	0.1	3.9

LEGENDS :

PERIOD CODE (IN SECONDS)
1= 4-5, 2= 6-7, 3= 8-9, 4= 10-11, 5= 12-13, 6= >13

WAVE HEIGHT CODE (IN METERS)
1= < 0.75, 2= 0.75-1.25, 3= 1.25-1.75, 4= 1.75-2.25, 5= 2.25-2.75,
6= 2.75-3.25, 7= 3.25-3.75, 8= 3.75-4.25, 9= >4.25

BAHAGIAN KEJURUTERAAN PANTAI
JABATAN PENGAIRAN DAN SALIRAN MALAYSIA
WAVE STATISTICS SUMMARIES - WAVE & SWELL

MARSDEN SQUARE : 2640 2650 2660 2748 2749 2756 2757 2758 2759 2766
2767 2768 2769
STARTING DATE : 01-01-1958 ENDING DATE : 31-12-1984
NO. OBSERVATIONS : 13481 PERCENT CALM : 0.00%
CHOSEN MONTHS : JAN FEB MAC APR MAY JUN JUL AUG SEP OCT NOV DEC

Direction : 225 - 255 DEGREES

	1	2	3	4	5	6	Total
1	2.4	0.0	0.0	0.0	0.0	0.0	2.5
2	1.2	0.1	0.1	0.0	0.0	0.0	1.5
3	0.4	0.2	0.1	0.0	0.0	0.0	0.6
4	0.2	0.1	0.0	0.0	0.0	0.0	0.3
5	0.0	0.0	0.0	0.0	0.0	0.0	0.1
6	0.0	0.0	0.0	0.0	0.0	0.0	0.1
7	0.0	0.0	0.0	0.0	0.0	0.0	0.0
8	0.0	0.0	0.0	0.0	0.0	0.0	0.0
9	0.0	0.0	0.0	0.0	0.0	0.0	0.0
Total	4.2	0.5	0.3	0.1	0.0	0.1	5.2

Direction : 255 - 285 DEGREES

	1	2	3	4	5	6	Total
1	4.6	0.1	0.0	0.0	0.0	0.1	4.9
2	2.8	0.5	0.2	0.0	0.0	0.1	3.6
3	1.1	0.5	0.1	0.0	0.0	0.0	1.9
4	0.4	0.2	0.1	0.0	0.0	0.0	0.8
5	0.1	0.2	0.1	0.0	0.0	0.0	0.4
6	0.1	0.1	0.0	0.0	0.0	0.0	0.2
7	0.0	0.0	0.0	0.0	0.0	0.0	0.1
8	0.0	0.0	0.0	0.0	0.0	0.0	0.0
9	0.0	0.0	0.0	0.0	0.0	0.0	0.1
Total	9.1	1.7	0.6	0.2	0.1	0.3	12.0

LEGENDS :

PERIOD CODE (IN SECONDS)
1= 4-5, 2= 6-7, 3= 8-9, 4= 10-11, 5= 12-13, 6= >13

WAVE HEIGHT CODE (IN METERS)
1= < 0.75, 2= 0.75-1.25, 3= 1.25-1.75, 4= 1.75-2.25, 5= 2.25-2.75,
6= 2.75-3.25, 7= 3.25-3.75, 8= 3.75-4.25, 9= >4.25

BAHAGIAN KEJURUTERAAN PANTAI
JABATAN PENGAIRAN DAN SALIRAN MALAYSIA
WAVE STATISTICS SUMMARIES - WAVE & SWELL

MARSDEN SQUARE : 2640 2650 2660 2748 2749 2756 2757 2758 2759 2766
2767 2768 2769
STARTING DATE : 01-01-1958 ENDING DATE : 31-12-1984
NO. OBSERVATIONS : 13481 PERCENT CALM : 0.00%
CHOSEN MONTHS : JAN FEB MAC APR MAY JUN JUL AUG SEP OCT NOV DEC

Direction : 285 - 315 DEGREES

	1	2	3	4	5	6	Total
1	5.8	0.4	0.1	0.1	0.0	0.1	6.5
2	4.8	1.2	0.3	0.1	0.0	0.2	6.6
3	1.9	1.2	0.3	0.1	0.0	0.1	3.5
4	0.5	0.6	0.1	0.0	0.0	0.1	1.4
5	0.2	0.2	0.1	0.0	0.0	0.0	0.4
6	0.0	0.0	0.0	0.0	0.0	0.0	0.1
7	0.0	0.0	0.0	0.0	0.0	0.0	0.1
8	0.0	0.0	0.0	0.0	0.0	0.0	0.0
9	0.1	0.0	0.0	0.0	0.0	0.0	0.1
Total	13.3	3.6	0.9	0.3	0.1	0.5	18.7

Direction : 315 - 345 DEGREES

	1	2	3	4	5	6	Total
1	4.4	0.2	0.0	0.0	0.0	0.1	4.8
2	2.8	0.7	0.2	0.0	0.0	0.1	3.8
3	0.8	0.5	0.1	0.0	0.0	0.1	1.5
4	0.2	0.3	0.0	0.0	0.0	0.0	0.5
5	0.0	0.1	0.0	0.0	0.0	0.0	0.1
6	0.0	0.0	0.0	0.0	0.0	0.0	0.1
7	0.0	0.0	0.0	0.0	0.0	0.0	0.0
8	0.0	0.0	0.0	0.0	0.0	0.0	0.0
9	0.0	0.0	0.0	0.0	0.0	0.0	0.1
Total	8.2	1.7	0.4	0.1	0.0	0.3	10.9

LEGENDS :

PERIOD CODE (IN SECONDS)
1= 4-5, 2= 6-7, 3= 8-9, 4= 10-11, 5= 12-13, 6= >13

WAVE HEIGHT CODE (IN METERS)
1= < 0.75, 2= 0.75-1.25, 3= 1.25-1.75, 4= 1.75-2.25, 5= 2.25-2.75,
6= 2.75-3.25, 7= 3.25-3.75, 8= 3.75-4.25, 9= >4.25

BAHAGIAN KEJURUTERAAN PANTAI
JABATAN PENGAIRAN DAN SALIRAN MALAYSIA
WAVE STATISTICS SUMMARIES - WAVE & SWELL

MARSDEN SQUARE : 2640 2650 2660 2748 2749 2756 2757 2758 2759 2766
2767 2768 2769
STARTING DATE : 01-01-1958 ENDING DATE : 31-12-1984
CHOSEN DIRECTION : 13481 PERCENT CALM : 0.00%
CHOSEN MONTHS : JAN FEB MAC APR MAY JUN JUL AUG SEP OCT NOV DEC

Number of observations in tables : 13481 Percentage : 100.00%

Reference : Mars2627.dbf
Processed by :
Date Processed : 29-05-2004
Fax Number :
Tel Number :
e-mail Address :